Electrical gate assisted optical multisubband spin-orbit control in GaInAs/AlInAs quantum wells with tilted nonresonant laser fields

Xue Li,[1,*] Yongmei Li,[1,2,*] Hao Yang,[1] Wen Liu,[2] Hailong Wang,[1] Ning Hao,[3] Jiyong Fu,[1,4,†] and Ping Zhang[1,5,‡]

[1]*Department of Physics, Qufu Normal University, 273165 Qufu, Shandong, China*

[2]*Department of Physics, Jining University, 273155 Qufu, Shandong, China*

[3]*Anhui Province Key Laboratory of Condensed Matter Physics at Extreme Conditions, High Magnetic Field Laboratory, HFIPS, Chinese Academy of Sciences, Hefei 230031, China*

[4]*Instituto de Física, Universidade de Brasília, Brasília-DF 70919-970, Brazil*

[5]*Beijing Computational Science Research Center, Beijing 100084, China*

(Received 11 September 2023; revised 26 November 2023; accepted 6 December 2023; published 21 December 2023)

Recently, we have proposed the concept of *laser-dressing-effect* mediated spin-orbit (SO) control in semiconductor wells, with the laser polarization aligning with the well-growth direction [X. Li *et al.*, Phys. Rev. B **106**, 155420 (2022)], facilitating flexible SO control. Here, for covering the full scenario and considering practical applications, we focus on *tilted* laser fields (TLFs) and build up a generic model incorporating both axial and transverse components of the laser polarization, which are respectively parallel and perpendicular to the well-growth direction, to explore the electrical gate assisted optical multisubband SO control in realistic GaInAs quantum wells with two occupied subbands. We reveal that the two laser components play contrasting roles in affecting SO properties from distinct physical sources, with the axial component directly altering the quantum confinement and the transverse component primarily adjusting the electron density of states. By performing a self-consistent Poisson-Schrödinger calculation (with both TLF and gate bias) in the Hartree approximation, we determine the full scenario of gate assisted TLF multisubband SO control, including intrasubband (Rashba α_ν and Dresselhaus β_ν) and intersubband (Rashba η and Dresselhaus Γ) types, $\nu = 1, 2$. Notably, we achieve adjusting the intrasubband Rashba α_1 and α_2 of the two subbands while meanwhile not only keeping them of opposite signs but also locking them to essentially equal strength, i.e., $\alpha_1 = -\alpha_2$, as a result of intertwined effect of the two laser components. This provides a *synchronous* symmetric Rashba control of distinct subbands, and facilitates the realization of persistent skyrmion lattice that we recently proposed [J. Fu *et al.*, Phys. Rev. Lett. **117**, 226401 (2016)], even with different pitches. Also, depending on the width of wells, we observe that α_1 can even be *pinned* at zero as TLF varies while α_2 can be flexibly adjusted, greatly fascinating for selective multisubband SO control in particular with suppressed spin relaxation for a given subband. As for the intrasubband Dresselhaus β_1 and β_2, which inherit the *bulk* nature of materials and thus are usually immune to electrical control, we unveil their flexible gate assisted optical tunability. Moreover, regarding the intersubband SO terms, while the Dresselhaus Γ is found weakly dependent on the TLF, the Rashba η is optically tunable and is even accompanied by a sign reversal. With the intersubband SO terms, we reveal three distinct scenarios for the spin-resolved multisubband dispersion, featuring the band crossing without spin hybridization and the band anticrossing with and without vertex corrections, respectively. Our work sheds light on experiments incorporating the TLF for a universal control of the Rashba-Dresselhaus SO terms of both intrasubband and intersubband kinds.

DOI: 10.1103/PhysRevB.108.235429

I. INTRODUCTION

Coherent control of spin is a prerequisite from fundamental physics to quantum information technology and spintronic devices. The spin-orbit (SO) interaction, which couples an electron spin and its orbital motion, acts on moving electrons as an effective magnetic field, enabling the manipulation of spin states *via* fully electrical means [1–3]. This essential idea has inspired various proposals on spintronic devices, e.g., spin-field [4–6] and spin-Hall effect transistors [7,8]. Also, the SO interaction underlies a plethora of novel physical phenomena such as the spin-orbit torque [9,10], spin galvanic effect [11], topological insulators [12], Majorana fermions [13–15], and Weyl semimetals [16]. Our recent proposals on persistent skyrmion lattice [17], stretchable spin helix [18,19], as well as helix-stretch based orbit (pseudospin) filter [20], which can be realized by fine tuning the SO strengths, also manifest the importance of SO effects for two-dimensional electron gases (2DEGs) hosted in semiconductor nanostructures.

For semiconductor 2DEGs, there are two dominant SO contributions: the Rashba [21] and the Dresselhaus [22] effects, arising from the breaking of structural and crystal inversion symmetries, respectively. The Rashba strength is essentially proportional to the external electric field exerting on 2DEGs, and thus can be tuned with the doping profile [23]

*These authors contributed equally to this work.

†yongjf@qfnu.edu.cn

‡zhang_ping@iapcm.ac.cn

as well as *in situ* using gate bias [24,25]. Extensive studies have been devoted to the Rashba coupling in semiconductor heterostructures with one [23,26–29] and even two [30–37] occupied subbands. Further, considering a triple quantum-well configuration, which favors electron occupation of the third subband, we unveiled intriguing Rashba SO control mediated by the charge transfer among distinct subwells [38]. In contrast to the Rashba coupling, the Dresselhaus coupling contains both linear and cubic terms, with the linear term mainly depending on the well confinement (e.g., well width) [23,39] and the cubic one on the electron density [18]. In addition, the interfacial effect in semiconductor heterostructures may also lead to an additional Dresselhaus term [3], which depends on the layer-dependent band parameters and can be comparable in magnitude to the usual linear term with both intrasubband and intersubband contributions [40]. The interfacial Dresselhaus term may provide an extra leverage for extracting reliable bulk Dresselhaus SO parameter, the value of which is usually controversial in both theory and experiment [3,41].

While an external gate bias is widely adopted for manipulating SO coupling [18,24,25], it certainly has limits in the control of Dresselhaus term, which embraces the intrinsic *bulk* nature of materials. As an effective way to complement electrical means, the SO manipulation and its measurement through optical manner have also gained growing interests [42–47]. In particular, the birth of ultrashort (from femtosecond to attosecond) laser pulses has made possible to produce intense light field, whose magnitude can even far exceed that of the atomic Coulomb field [48,49]. As a consequence, the light, which had long been used only as a probe for matter, has now achieved such huge intensity that the electronic states bound in atoms, molecules, clusters, and solids could be strongly modified [48,49]. These modified states are the so-called laser-*dressed* electronic states (or potentials) [48–53], originating from the optical stark effect.

With the advent of high-quality and tunable laser sources (e.g., free-electron lasers), the *dressing* effect of intense high-frequency laser (IHFL) fields has exhibited strong experimental evidences and has been widely adopted in various experiments and applications, including atomic stabilization [50], molecular dissociation [51], and higher-order harmonic generation [54]. More interestingly, in the case of semiconductor heterostructures, the IHFL field was found dressing quantum confining potential and greatly altering the quantized energy levels. This gives rise to intriguing control of electronic and optical properties of 2DEGs [52,55–57]. And, recently, we have first proposed the concept of laser-dressing-effect mediated spin-orbit (SO) control in semiconductor wells, with the laser polarization aligning with the well-growth direction [43], facilitating flexible SO control.

In reality, the applied laser field may usually have both perpendicular (axial) and parallel (transverse) components of the polarization. And, depending on the incident light polarization, strong anisotropy of the optical and magnetic properties usually occurs [58,59]. However, most studies on intense laser fields were devoted to the special case of laser polarization aligning with the growth ($z \parallel [001]$) direction of quantum wells [43,52,55–57], i.e., solely with the axial component. Further, so far, how the laser transverse component affects SO

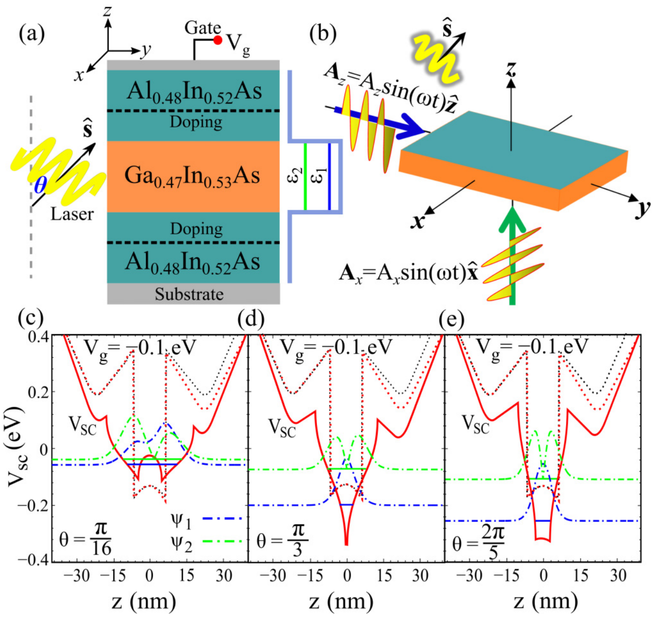

FIG. 1. (a) Schematic diagram of a $Al_{0.48}In_{0.52}As/Ga_{0.47}In_{0.53}As/Al_{0.48}In_{0.52}As$ quantum well subjected to an external gate bias (V_g) and *tilted* laser field (TLF), with θ the tilt angle between the laser polarization ($\hat{\mathbf{s}}$) and the well-growth direction (z axis). The dashed (black) regions inside the barrier ($Al_{0.48}In_{0.52}As$) layers represent the dopants with a symmetric doping condition, and $\mathcal{E}_1$ ($\mathcal{E}_2$) stands for the energy level of the first (second) subband. (b) Illustration of TLF, with the laser propagation along the y (blue arrow) and z (green arrow) axes, corresponding to the polarization parallel to the z ($\mathbf{A}_z$; axial component) and x ($\mathbf{A}_x$; transverse component) directions, respectively. [(c)–(e)] Self-consistent potential V_{sc} and wave functions ψ_ν ($\nu = 1, 2$) of the two subbands for the well of width $L_w = 13$ nm at $V_g = -0.1$ eV, with the tilt angle $\theta = \pi/16$ (c), $\pi/3$ (d), and $2\pi/5$ (e). The horizontal blue (green) line inside the well indicates the self-consistent energy level $\mathcal{E}_1$ ($\mathcal{E}_2$), and the dotted red (black) curve refers to V_{sc} without TLF (without both TLF and V_g).

properties remains unknown, let alone its *intertwined* effect with the laser axial component. Therefore, considering restrictions for a universal and simultaneous control of Rashba and Dresselhaus of both intrasubband and intersubband types, we believe it is greatly desired to construct a generic and comprehensive model taking into account both aspects of the laser axial and transverse components and explore the intertwined effect of the two components (together with electrical means) on SO properties, not only for the fundamental theoretical value, but also for practical applications, where manipulating SO is important to control spin and engineer devices.

Here, for covering the full scenario of SO control and considering practical applications, we focus on *tilted* laser fields (TLFs) [Fig. 1(a)] and build up a generic model incorporating both axial and transverse components of the laser polarization, which are respectively parallel and perpendicular to the well-growth direction [Fig. 1(b)], to explore the electrical gate assisted optical multisubband SO control in realistic GaInAs quantum wells with two occupied subbands.We reveal that the two laser components may play contrasting roles in affecting SO properties from distinct physical sources, with the axial component directly altering the quantum confinement and the transverse component primarily adjusting the electron density of states. Also, by accounting for SO contributions from both TLFs and gate bias, we derive an effective 4×4 Rashba and Dresselhaus Hamiltonian (two for each subband) for conduction electrons, with all the relevant SO terms of both intrasubband (Rashba α_ν and Dresselhaus β_ν, $\nu = 1, 2$) and intersubband (Rashba η and Dresselhaus Γ) types. We consider quantum wells that are similar to the experimental samples of Ref. [60], while with two occupied electron subbands for covering both the intrasubband and intersubband SO contributions. By self-consistently solving the Schrödinger and Poisson equations (with both TLF and gate bias) for 2DEGs in the Hartree approximation, we systematically determine the gate assisted TLF multisubband SO control. For completeness, we consider both relatively narrow and relatively wide wells, of the well width equal to 13 and 26 nm, respectively, since narrow and wide quantum wells may exhibit contrasting SO features [61].

Remarkably, we achieve adjusting the intrasubband Rashba α_1 and α_2 of the two subbands while meanwhile not only keeping them of opposite signs but also locking them to essentially equal strength, i.e., $\alpha_1 = \alpha_2$, as a result of intertwined effect of the two components of the laser polarization. This provides a *synchronous* symmetric Rashba SO control of distinct subbands, and facilitates the realization of persistent skyrmion lattice (i.e., *crossed* spin helices) that we recently proposed [17], even with different pitches (spin-density wave length), which depends on SO strengths. Also, depending on the width of quantum wells, we observe that α_1 can even be locked to zero as the TLF varies while α_2 can be flexibly adjusted, greatly fascinating for selective multisubband SO control in particular with suppressed spin relaxation for a given subband. As for the intrasubband Dresselhaus β_1 and β_2, which inherit the *bulk* nature of materials and thus are usually immune to electrical control, we unveil their flexible gate assisted optical tunability. Moreover, regarding the intersubband SO terms, while the Dresselhaus Γ is found weakly dependent on the TLF, the Rashba η is optically tunable even accompanied by a sign reversal. With the intersubband SO terms, we reveal three distinct scenarios for the multisubband spin-resolved dispersion, featuring the band crossing without spin hybridyzation and the band anticrossing with and without vertex corrections of the spin texture, respectively. Our work sheds light on experiments incorporating the TLF for a universal control of the Rashba-Dresselhaus SO terms of both intrasubband and intersubband kinds.

The paper is organized as follows. In Sec. II, we present our theoretical framework of the laser-dressed potential and the laser-modified DOS for 2DEGs, following approaches of Floquet theory [48] and averaged Green's functions [57], respectively. Then, by accounting for SO contributions from both TLFs and gate bias, we derive an effective two-dimensional (2D) model with two occupied electron subbands, i.e., 4×4 SO Hamiltonian (two for each subband), from the three-dimensional (3D) Hamiltonian accounting for the Rashba and Dresselhaus couplings. Also, we present the expressions of the Rashba and Dresselhaus SO terms of both intrasubband and intersubband kinds. In Sec. III, we introduce our quantum system and the involved parameters. In Sec. IV, we show the self-consistent results, and discuss in detail the electrical gate assisted optical multisubband SO control with both the axial and transverse components of the laser polarization. The impact of the intersubband terms on the spin-resolved multisubband energy dispersion, which involves the band crossing and the band avoided crossing with and without vertex correction of the spin texture, is also discussed. We summarize our main findings in Sec. V.

II. THEORETICAL FRAMEWORK

In this section, we first focus on the laser-dressing effects of the two (axial and transverse) components of TLF on electronic states in quantum wells. Then, we take into account SO contributions from both TLF and gate bias, and derive an effective 2D electron Hamiltonian for quantum wells with two subbands, containing both Rashba and Dresselhaus SO couplings of the intrasubband and intersubband types, from the 3D form of the Hamiltonian. The expressions for all the relevant intrasubband and intersubband SO terms including the corresponding SO strengths are also presented.

A. Electronic states in quantum wells with TLF

Considering contrasting impacts of the two laser components on 2D electrons, we resort to different theoretical approaches to model them. Specifically, to describe the laser-dressing effect of the axial component, we follow the Floquet approach [48], while to unveil the effect of the transverse component, we adopt the method of averaged Green's functions [57]. Below we analyze in detail the laser-dressed potential and the laser-modified DOS for 2DEGs, primarily due to the axial and transverse components of the laser polarization, respectively.

1. Laser-dressed potential

To describe the motion of electrons in the presence of light field, the radiation field under the dipole approximation can be described by the plane wave, i.e., $\mathbf{A}(t) = A\ \sin(\omega t)(\hat{\mathbf{x}}\ \sin\theta + \hat{\mathbf{z}}\ \cos\theta)$, with θ the tilt angle between the polarization of laser field and the growth direction of quantum well, A the potential amplitude, and ω the laser radiation angular frequency. Here, the two components, i.e., $\mathbf{A}_z(t) = A\ \cos\theta\ \sin(\omega t)\hat{\mathbf{z}}$ and $\mathbf{A}_x(t) = A\ \sin\theta\ \sin(\omega t)\hat{\mathbf{x}}$, which are perpendicular to each other, are along the axial (parallel to the z axis) and transverse (parallel to the x axis) directions, respectively [Figs. 1(a) and 1(b)]. In the following, for simplifying notations, we define $A_z = A\ \cos\theta$ and $A_x = A\ \sin\theta$, separately referring to the laser electric field strengths of $F_z = A_z\omega$ and $F_x = A_x\omega$.

By applying the Kramers-Henneberger space-translation transformation and taking into account the space-translated version of the time-dependent Schrödinger equation for 2DEGs subjected to laser fields, one obtains [62–67]

$$\left[\frac{1}{2m^*}(\mathbf{p} - e\mathbf{A}_\mu)^2 + V_{\mathrm{w}}(z)\right]\Psi(\mathbf{r}, t) = i\hbar\frac{\partial\Psi(\mathbf{r}, t)}{\partial t}, \qquad (1)$$

where $\mathbf{p} = -i\hbar\nabla$ is the momentum operator, e represents the electron charge, and μ $(= z, x)$ denotes the axis index.

The laser-dressed potential energy is mainly caused by the axial component $\mathbf{A}_z(t)$, which can be manifested by a unitary transformation $\Psi(\mathbf{r},t) \longrightarrow \phi(\mathbf{r},t)$ [68,69]. Accordingly, Eq. (1) is rewritten as

$$\left[-\frac{\hbar^2}{2m^*}\nabla^2 + \widetilde{V}_{\mathrm{w}}(z+\alpha_z(t))\right]\phi(z,t) = i\hbar\frac{\partial}{\partial t}\phi(z,t), \quad (2)$$

where $\widetilde{V}_{\mathrm{w}}[z+\alpha_z(t)]$ is the so-called laser-dressed potential energy. Here we have defined $\alpha_z(t) = \alpha_z\cos(\omega t)\hat{\mathbf{z}}$ the displacement vector of the electron due to its quiver motion in the presence of laser field, with $\alpha_z \equiv eA_z/(m^*c\omega)$ (c the light speed) the axial laser parameter.

Following the Floquet approach [48], the time-dependent Schrödinger equation [Eq. (2)] can be transformed into the coupled time-independent differential equations in terms of Floquet component of the wave function ϕ, where the Floquet state is the analog to a Bloch state when replacing a spatially periodic potential to a time-periodic one. To solve the coupled differential equations, an iteration scheme, which essentially proceeds in inverse powers of ω, can be adopted. Up to the lowest order in ω, i.e., in the high-frequency limit of $\omega\tau \gg 1$ with τ the transit time of electrons [66,70], the photon absorption by the system becomes essentially impossible [48,71], greatly quenching thermal effect. And, in this case, the set of coupled equations reduces to a single one [48,67,71],

$$\left[-\frac{\hbar^2}{2m^*}\nabla^2 + \widetilde{V}_{\mathrm{w}}(z;\alpha_z)\right]\phi_0(z) = E\phi_0(z), \quad (3)$$

with ϕ_0 the zeroth Floquet component and $\widetilde{V}_{\mathrm{w}}(z;\alpha_z)$ the laser-dressed potential energy [72], which is determined by the axial laser parameter α_z associated with the laser intensity I and the laser oscillation frequency ω. And, depending on the value of α_z, there exist two distinct regimes for the laser-dressed potential energy, marked at $\alpha_z = L_{\mathrm{w}}/2$ (i.e., half of the well width). Specifically, when $\alpha_z \leqslant L_{\mathrm{w}}/2$,

$$\widetilde{V}_{\mathrm{w}}(z;\alpha_z) = \frac{\delta_c}{\pi}\left[\Theta(\alpha_z - L_{\mathrm{w}}/2 - z)\arccos\left(\frac{L_{\mathrm{w}}/2+z}{\alpha_z}\right) + \Theta(\alpha_z - L_{\mathrm{w}}/2 + z)\arccos\left(\frac{L_{\mathrm{w}}/2-z}{\alpha_z}\right)\right], \quad (4)$$

and when $\alpha_z > L_{\mathrm{w}}/2$,

$$\begin{aligned}\widetilde{V}_{\mathrm{w}}(z;\alpha_z) &= \frac{\delta_c}{\pi}\Bigg\{\Theta(L_{\mathrm{w}}/2 - \alpha_z - z)\arccos\left(\frac{L_{\mathrm{w}}/2+z}{\alpha_z}\right) \\ &+ \Theta(L_{\mathrm{w}}/2 - \alpha_z + z)\arccos\left(\frac{L_{\mathrm{w}}/2-z}{\alpha_z}\right) \\ &+ [\Theta(z - L_{\mathrm{w}}/2 + \alpha_z) + \Theta(-z - L_{\mathrm{w}}/2 + \alpha_z) - 1] \\ &\times \left[\pi + \arcsin\left(\frac{z - L_{\mathrm{w}}/2}{\alpha_z}\right) - \arcsin\left(\frac{z + L_{\mathrm{w}}/2}{\alpha_z}\right)\right]\Bigg\}, \end{aligned} \quad (5)$$

where δ_c stands for the barrier height of quantum wells, Θ denotes the Heaviside step function, and L_{w} is the well width. Clearly, at zero laser parameter ($\alpha_z = 0$), the laser-dressed potential $\widetilde{V}_{\mathrm{w}}(z;\alpha_z)$ will recover the original square potential $[V_{\mathrm{w}}(z)]$ for confining electrons, in either case of $\alpha_z \leqslant L_{\mathrm{w}}/2$ or $\alpha_z > L_{\mathrm{w}}/2$, namely, $\widetilde{V}_{\mathrm{w}}(z;\alpha_z) \to V_{\mathrm{w}}(z)$ as $\alpha_z \to 0$, with $V_{\mathrm{w}}(z) = \delta_c[\Theta(z - L_{\mathrm{w}}/2) + \Theta(-z - L_{\mathrm{w}}/2)]$. Note that Eqs. (4) and (5) essentially involve the transition from a usual single well to an effective double well, entirely arising from the laser-dressing effect, as we will emphasize later on in Sec. IV.

2. Laser-modified DOS

The effect of the transverse component $\mathbf{A}_x(t)$ of the laser polarization on electronic states can be obtained by directly integrating Eq. (1) over t for $\mathbf{A}_x(t) = A_x\sin(\omega t)\hat{\mathbf{x}}$. This yields the time-dependent wave function

$$\begin{aligned}\Psi_{\nu,\mathbf{k}}(\mathbf{r},t) &= \Psi_{\nu,\mathbf{k}}(\mathbf{r},0)\exp\{-\mathrm{i}/\hbar[\mathrm{E}_\nu(\mathbf{k}) + 2\gamma\hbar\omega]\mathrm{t}\} \\ &\times \exp\{\mathrm{i}\alpha_x k_x[1-\cos(\omega t)]\}\exp[\mathrm{i}\gamma\ \sin(2\omega t)],\end{aligned} \quad (6)$$

where $\Psi_{\nu,\mathbf{k}}(\mathbf{r},0) = e^{i\mathbf{k}\cdot\mathbf{r}}\psi_\nu(z)$, $\gamma \equiv e^2A_x^2/8m^*\hbar\omega$ (dimensionless), $\alpha_x \equiv eA_x/(m^*c\omega)$ is the transverse laser parameter, and $2\gamma\hbar\omega = e^2F_x^2/4m^*\omega^2$ stands for the energy blueshift induced by the transverse component. The wave function in Eq. (6) determines the probability amplitude $P_{|\nu',\mathbf{k}'\rangle\to|\nu,\mathbf{k}\rangle}$ of the process for an electron in a state $|\nu',\mathbf{k}'\rangle$ at time t' evolving into another state $|\nu,\mathbf{k}\rangle$ at time t, which reads as

$$\begin{aligned}P_{|\nu',\mathbf{k}'\rangle\to|\nu,\mathbf{k}\rangle} &= \int \Psi^*_{\nu',\mathbf{k}'}(\mathbf{r},t')\Psi_{\nu,\mathbf{k}}(\mathbf{r},t)d^3 \\ r &= h_{\nu,\mathbf{k}}(t,t')\delta_{\nu,\nu'}\delta_{\mathbf{k},\mathbf{k}'},\end{aligned} \quad (7)$$

with

$$\begin{aligned}h_{\nu,\mathbf{k}}(t,t') &= \exp\{-\mathrm{i}/\hbar[\mathrm{E}_\nu(\mathbf{k}) + 2\gamma\hbar\omega](\mathrm{t}-\mathrm{t}')\} \\ &\times \exp\{-\mathrm{i}\alpha_x k_x[\cos(\omega t) - \cos(\omega t')]\} \\ &\times \exp\{\mathrm{i}\gamma[\sin(2\omega t) - \sin(2\omega t')]\}.\end{aligned} \quad (8)$$

For noninteracting electrons, the Green's function is $G^+_{\nu,\mathbf{k}}(t > t') = -i/\hbar\Theta(t-t')h_{\nu,\mathbf{k}}(t,t')$ [73], which is the solution of

$$\left[\mathcal{E}_\nu + \frac{(\hbar\mathbf{k} - e\mathbf{A}_x)^2}{2m^*} - i\hbar\frac{\partial}{\partial t}\right]G^+_{\nu,\mathbf{k}}(t > t') = \delta(t'-t) \quad (9)$$

in the $(\nu,\mathbf{k};t)$ space, and

$$\begin{aligned}&\left[\frac{(\mathbf{p} - e\mathbf{A}_x)^2}{2m^*} + V_{\mathrm{w}}(z) - i\hbar\frac{\partial}{\partial t}\right]G^+_{\nu,\mathbf{k}}(t > t')\Psi_{\nu,\mathbf{k}}(\mathbf{r},0) \\ &= \delta(t'-t)\Psi_{\nu,\mathbf{k}}(\mathbf{r},0)\end{aligned} \quad (10)$$

in the real space. The Fourier transform of the retarded Green's function reads as

$$G^+_{\nu,\mathbf{k}}(E,t') = \int_{-\infty}^{+\infty}\exp[\mathrm{i}/\hbar(\mathrm{E} + \mathrm{i}\eta)\tau]G^+_{\nu,\mathbf{k}}(\mathrm{t} > \mathrm{t}')d\tau, \quad (11)$$

where $\tau = t - t'$, and $i\eta$ is the infinitesimal to avoid divergences. Then, with the help of Bessel functions, Eq. (11) can be rewritten as

$$G^{+}_{\nu,\mathbf{k}}(E,t') = \sum_{m=-\infty}^{+\infty} \frac{\widetilde{F}_m(k_x,t')}{E - E_\nu(\mathbf{k}) - 2\gamma\hbar\omega - m\hbar\omega + i\eta}, \quad (12)$$

where $\widetilde{F}_m(k_x,t')$ is the auxiliary function,

$$\widetilde{F}_m(k_x,t') \equiv (-1)^m F_m(k_x) \sum_{\ell=-\infty}^{+\infty} i^\ell J_{m+\ell}(\alpha_x k_x) \times \exp\{\mathrm{i}[\ell\omega \mathrm{t}' - \gamma \sin(2\omega \mathrm{t}')]\}, \quad (13)$$

with $J_m(x)$ the Bessel function and

$$F_m(k_x) = \sum_{q=0}^{\infty} \frac{J_q(\gamma)}{1+\delta_{q,0}}[J_{2q-m}(\alpha_x k_x) + (-1)^{m+q} J_{2q+m}(\alpha_x k_x)]. \quad (14)$$

By averaging t' over one period of laser fields [74] in Eq. (12), one can obtain the steady-state properties, with the averaged Green's function being written as

$$G^{*}_{\nu,\mathbf{k}}(E) = \sum_{m=-\infty}^{+\infty} \frac{F_m^2(k_x)}{E - E_\nu(\mathbf{k}) - 2\gamma\hbar\omega - m\hbar\omega + i\eta}. \quad (15)$$

Thus, under the impact of the transverse component (α_x) of the laser polarization, the usual *constant* 2D DOS for electrons occupying the νth subband, i.e., $D_\nu(E) = \rho_0 \equiv m^*/(\pi\hbar^2)$, needs to be modified. And, the modified DOS can be determined from the imaginary part of the averaged Green's function, with $D_\nu(E) = -2/\pi \sum_{\mathbf{k}} \mathrm{Im}\{\mathrm{G}^*_{\nu,\mathbf{k}}(\mathrm{E})\}$, which in a more expanded form reads as

$$D_\nu(E) = \frac{2}{\pi}\rho_0 \sum_{m=0}^{\infty} \Theta(\overline{E}_{\nu\gamma m}) \int_0^1 \frac{d\xi}{\sqrt{1-\xi^2}} F_m^2\left(\xi \frac{\sqrt{2m^*\overline{E}_{\nu\gamma m}}}{\hbar}\right), \quad (16)$$

where $\overline{E}_{\nu\gamma m} \equiv E - \mathcal{E}_\nu - 2\gamma\hbar\omega - m\hbar\omega$. In terms of the nonresonant laser beam, only nonresonant photons join in the optical process, and thus no absorption and emission processes are allowed. This causes that only the term corresponding to $m = 0$ in Eq. (16) will survive, and thus the summation in Eq. (16) is reduced to

$$D_\nu(E) = \frac{2}{\pi}\rho_0 \Theta(E - \mathcal{E}_\nu - 2\gamma\hbar\omega) \times \int_0^1 \frac{d\xi}{\sqrt{1-\xi^2}} F_0^2\left(\xi \frac{\sqrt{2m^*(E - \mathcal{E}_\nu - 2\gamma\hbar\omega)}}{\hbar}\right), \quad (17)$$

where $F_0(k_x) = J_0(\gamma)J_0(\alpha_x k_x) + 2\sum_{q>0,\mathrm{even}} J_q(\gamma)J_{2q}(\alpha_x k_x)$. The laser-modified DOS depends on both the laser field strength and frequency through the parameters γ and α_x. When the strength of the transverse component of TLF is lower and (or) the frequency of TLF is higher, one has $\gamma \to 0$ and $\alpha_x \to 0$, thus, $F_0(k_x) \to 1$ since $J_q(0) = \delta_{q,0}$. Clearly, in this case, the laser-modified DOS recovers its usual ladder profile appearing in the case without laser fields.Note that, for a realistic laser source, the laser parameter $\alpha_\mathrm{L} (= \sqrt{\alpha_z^2 + \alpha_x^2})$ depends on its intensity I and frequency ω, which can be expressed as $\alpha_\mathrm{L} = (I^{1/2}/\omega^2)(e/m^*)(8\pi/c)^{1/2}$ [43]. Thus, as long as θ is fixed, the laser-dressed potential energy and laser-modified DOS are determined by ω and I through α_L.

B. Model Hamiltonians: From 3D to 2D

Here we show the derivation of an effective 2D model from a 3D Hamiltonian involving Rashba and Dresselhaus SO couplings, and present the concrete expressions of intrasubband and intersubband terms in the case of two subbands. For intrasubband Dresselhaus coefficients, we also give the expressions of its cubic term $\beta_{\nu,3}$ and renormalized term $\beta_{\nu,\mathrm{eff}}$.

1. 3D SO Hamiltonian

We consider GaInAs/AlInAs quantum wells grown along the $z \parallel (001)$ direction. Based on the 8×8 Kane model involving conduction and valence bands, an effective 3D SO Hamiltonian for electrons reads as [61,75],

$$\mathcal{H}^{3\mathrm{D}} = \frac{\hbar^2 k^2}{2m^*} - \frac{\hbar^2}{2m^*}\frac{\partial^2}{\partial z^2} + V_{\mathrm{sc}}(z) + \mathcal{H}_R^{3\mathrm{D}} + \mathcal{H}_D^{3\mathrm{D}}, \quad (18)$$

where $m^* = 0.043m_0$ (m_0 the bare electron mass) is the effective electron mass and k is the in-plane electron momentum. The third term $V_{\mathrm{sc}} = V_\mathrm{w} + V_\mathrm{g} + V_\mathrm{L} + V_\mathrm{d} + V_\mathrm{e}$ refers to the total electron confining potential with self-consistence, which is determined within the Schrödinger and Poisson equations in the Hartree approximation, with V_w the structural potential arising from the band offset, V_g the external gate potential, V_L the external laser field potential, V_d the doping potential, and V_e the electronic Hartree potential [17,18,37,61]. The last two terms $\mathcal{H}_R^{3\mathrm{D}}$ and $\mathcal{H}_D^{3\mathrm{D}}$ describe Rashba and Dresselhaus SO interactions, respectively. For Rashba term, $\mathcal{H}_R^{3\mathrm{D}} = \eta(z)(k_x\sigma_y - k_y\sigma_x)$, where $\eta(z) = \eta_\mathrm{w}\partial_z V_\mathrm{w} + \eta_\mathrm{H}\partial_z(V_\mathrm{g} + V_\mathrm{d} + V_\mathrm{e} + V_\mathrm{L})$ determines the Rashba coupling strength, and $\sigma_{x,y,z}$ are the spin Pauli matrices. The parameters η_w and η_H are connected with the bulk quantities of materials [37,61,76]. And for Dresselhaus term, $\mathcal{H}_D^{3\mathrm{D}} = \gamma[\sigma_x k_x(k_y^2 - k_z^2) + \mathrm{c.p.})]$, where γ is the bulk Dresselhaus parameter and $k_z = -i\partial_z$ [22,75]. Further, expanding on $\mathcal{H}_D^{3\mathrm{D}}$, we get the cubic contribution $\mathcal{H}_{D(3)}^{3\mathrm{D}} = \gamma k_x k_y(\sigma_x k_y - \sigma_y k_x)$.

2. Effective 2D model

Now we are ready to derive an effective 2D model starting from the 3D Hamiltonian [Eq. (18)]. First, we determine (self-consistently) the spin-degenerate eigenspinors $|\mathbf{k}\nu\sigma\rangle = |\mathbf{k}\nu\rangle \otimes |\sigma\rangle$, $\langle \mathbf{r}|\mathbf{k}\nu\rangle = \exp(i\mathbf{k}\cdot\mathbf{r})\psi_\nu(z)$ and eigenvalues $\varepsilon_{\mathbf{k}\nu} = \mathcal{E}_\nu + \hbar^2k^2/2m^*$ ($\nu = 1, 2$) of quantum wells without SO interaction. Here, $\mathcal{E}_\nu$ (ψ_ν) is defined as the νth quantized energy level (wave function), $\mathbf{k}$ is the in-plane wave vector, and $\sigma = (\uparrow, \downarrow)$ is the electron spin component along the z direction. Then, by projecting Eq. (18) onto the spin-degenerate basis set $\{|\mathbf{k}\nu\sigma\rangle\}$, we obtain the effective 2D model for the Rashba and Dresselhaus SO couplings in quantum wells with two occupied electron subbands having both intrasubband and intersubband terms. Under the coordinate system $[x \parallel (100), y \parallel (010)]$ with the basis set $\{|\mathbf{k}1\uparrow\rangle, |\mathbf{k}1\downarrow\rangle, |\mathbf{k}2\uparrow\rangle, |\mathbf{k}2\downarrow\rangle\}$, our effective 2D model with two subbands reads as

$$\mathcal{H}^{2D} = \begin{pmatrix} \rho_{11} & \rho_{12} \\ \rho_{21} & \rho_{22} \end{pmatrix}, \quad (19)$$

where $\rho_{\nu\nu} = \varepsilon_{\mathbf{k}\nu}\mathbb{1} + \alpha_\nu(\sigma_y k_x - \sigma_x k_y) + \beta_\nu(\sigma_y k_y - \sigma_x k_x)$, $\nu = 1, 2$, $\rho_{12} = \eta(\sigma_y k_x - \sigma_x k_y) + \Gamma(\sigma_y k_y - \sigma_x k_x)$, and $\rho_{21} = \rho_{12}^\dagger$, with $\mathbb{1}$ the 2×2 matrix in both spin and orbital (subband) subspaces, $\sigma_{x,y}$ the spin Pauli matrices, $k_{x,y}$ the wave vector components along the $x \parallel \langle 100\rangle$ and $y \parallel \langle 010\rangle$ directions. The parameters α_ν (η) and β_ν (Γ) are intrasubband (intersubband) Rahsba and Dresselhaus SO coefficients.

C. Multisubband Rashba and Dresselhaus SO coefficients: Both intrasubband and intersubband types

The Rashba SO coefficients appearing in Eq. (19) can be expressed as the matrix elements $\langle\dots\rangle$ of the weighted derivatives of the potential contributions,

$$\eta_{\nu\nu'} = \langle\psi_\nu|\eta_w\partial_z V_w + \eta_H\partial_z(V_g + V_L + V_d + V_e)|\psi_{\nu'}\rangle, \quad (20)$$

with the intrasubband (intersubband) Rashba coefficients $\alpha_\nu \equiv \eta_{\nu\nu}$ ($\eta \equiv \eta_{12}$). Here the intrasubband Rashba term α_ν can be expressed as the sum of several constituent contributions, i.e., $\alpha_\nu = \alpha_\nu^g + \alpha_\nu^L + \alpha_\nu^d + \alpha_\nu^e + \alpha_\nu^w$, with $\alpha_\nu^g = \eta_H\langle\psi_\nu|\partial_z V_g|\psi_\nu\rangle$ the gate contribution, $\alpha_\nu^L = \eta_H\langle\psi_\nu|\partial_z V_L|\psi_\nu\rangle$ the laser field contribution, $\alpha_\nu^d = \eta_H\langle\psi_\nu|\partial_z V_d|\psi_\nu\rangle$ the doping contribution, $\alpha_\nu^e = \eta_H\langle\psi_\nu|\partial_z V_e|\psi_\nu\rangle$ the electron Hartree contribution, and $\alpha_\nu^w = \eta_w\langle\psi_\nu|\partial_z V_w|\psi_\nu\rangle$ the structural contribution. Similarly, the intersubband Rashba term $\eta = \eta^g + \eta^L + \eta^d + \eta^e + \eta^w$. For convenience, we also mark $\alpha_\nu^{g+d}(\eta^{g+d}) = \alpha_\nu^g(\eta^g) + \alpha_\nu^d(\eta^d)$. In addition, we should emphasize that, for simplifying notations in our model, we treat the laser field contribution as follows: (i) even though the ingredient α_ν^L denotes the laser field contribution, it is mainly dominated by the laser axial component, which gives rise to modifications to the original structural (square-well) potential (V_w) through the laser-dressed one ($\widetilde{V}_w$) (Sec. II A 1); (ii) the effect of the laser transverse component is encoded in all the ingredient contributions α_ν^e, α_ν^g, α_ν^d, α_ν^w, and even α_ν^L, through our self-consistent subband wave functions ψ_ν determined by the corresponding potential energies of V_e, V_g, V_d, V_w, and V_L.

The Dresselhaus SO coefficients read as

$$\Gamma_{\nu\nu'} = \gamma\langle\psi_\nu|k_z^2|\psi_{\nu'}\rangle, \quad (21)$$

with the intrasubband (intersubband) Dresselhaus coefficients $\beta_\nu \equiv \Gamma_{\nu\nu}$ ($\Gamma \equiv \Gamma_{12}$). In particular, for β_ν, we extend a renormalized term by defining $\beta_{\nu,\mathrm{eff}} = \beta_\nu - \beta_{\nu,3}$, with the cubic term $\beta_{\nu,3} = \gamma k_F^2/4$, where $k_F \simeq \sqrt{2\pi n}$ is the Fermi wave vector with n being the areal electron density.

For realistic wells, both the Rashba (α_ν) and Dresselhaus (β_ν) couplings always depend on the overall response of the gate potential V_g, the laser field potential V_L, the doping potential V_d, the electron Hartree potential V_e, and the structural potential V_w. They are not solely dependent on the external gate or laser field. That is, for each value of V_g, α_z, and α_x, the total confining potential $V_{sc} = V_w + V_g + V_L + V_d + V_e$ and the eigenenergy and corresponding wave function of the system are recalculated self-consistently before the relevant SO coefficients [Eqs. (20) and (21)] are determined.

III. SYSTEM AND RELEVANT PARAMETERS

We consider ordinary $Ga_{0.47}In_{0.53}As/Al_{0.48}In_{0.52}As$ quantum wells of width L_w grown along the $z \parallel [001]$ direction [Fig. 1(a)], similar to the experimental sample of Refs. [60,61,77] while with two occupied subbands for electrons. The quantum wells are exposed to both an external gate bias (V_g) and tilted IHFL field characterized by the tilt angle θ with respect to the well-growth direction [Fig. 1(a)]. The laser field is taken to propagate along the y axis, and accordingly the axial (A_z) and transverse (A_x) components of the laser polarization are along the z and x axes [Fig. 1(b)], respectively. These considerations on our quantum wells allow for gate assisted optical multisubband SO control, through not only the laser parameter (α_z; α_x) determined by the laser intensity, but also the tilt angle θ of the laser polarization. Specifically, the gate bias is utilized for a simultaneous tuning of the electron subband occupancy and the structural inversion asymmetry (SIA) of the system, while the tilted laser field is used to *dress* the quantum confinement potential and alter the quantized subband energy levels as well as the DOS of electrons.

In order to capture complete features of the gate assisted optical multisubband SO control, we consider both relatively narrow and relatively wide quantum wells, of the width L_w = 13 and 26 nm, respectively. For our wells, two symmetric doping layers of width 6 nm in $Al_{0.48}In_{0.52}As$ barrier layers sit 13 nm away from either side of the well with the same doping density $\rho = 4\times10^{18}$ cm^{-3}, ensuring that the well at zero gate bias ($V_g = 0$) is structurally symmetric (i.e., lack of SIA). The band offset δ_c at the $Ga_{0.47}In_{0.53}As/Al_{0.48}In_{0.52}As$ interfaces is chosen as 0.52 eV [37,78]. In our self-consistent Poisson-Schrödinger calculation, the Fermi level E_F, with which one can adjust the subband occupations, is pinned at $E_F = 0$ to ensure that the system sustains the condition of double-electron occupancy [18,40]. Note that the Fermi level is readily tunable in experiments, e.g., through electrical means [79,80]. The temperature is 0.3 K, and the thermal effect, which favors the electron occupation of higher-energy subbands at elevated temperatures, is mainly encoded in the Fermi-Dirac distribution appearing in our self-consistent procedure [18,37,61]. Strictly speaking, although the band parameters and the Kane parameters involved in the Kane model also depend on temperature, we have recently verified that these effects only provide negligible corrections to the SO couplings [81]. Therefore, our results about SO properties are essentially also valid for temperatures above 0.3 K within a regime that the higher third subband remains unoccupied. When the third subband starts to be occupied by electrons, there will be more emerging SO contributions of intrasubband and intersubband kinds [38].

For the IHFL field, on the one hand, the high-frequency regime mentioned above in general implies that the condition of $\omega\tau \gg 1$ satisfies [70], with $\tau \sim$ ps the transit time of electrons, so that the electron is not capable of feeling the rapidly oscillating potential, namely, the electron could *see* an evident laser-dressing effect. The frequency in such regime could range from several to even thousands of THz, depending on specific applications [82,83]. On the other hand, here we mainly focus on the SO properties without optical transitions, and hence consider the laser frequency tuned to be off resonant with both intersubband (c-c for conduction band-conduction band) and interband (c-v for conduction band-valence band, i.e., the band gap) transitions. For our wells, the energy separations of the intersubband (c-c) and interband (c-v) transitions are about 100 and 816 meV [78], which correspond to the resonant frequencies of about 25 and 200 THz, respectively. Thus, we consider a reasonable value of the frequency of $\omega/(2\pi) = 1.5$ THz (far less than the c-c and c-v resonance energies) and the laser electric field strength of $F = 2.5$ kV/cm. These considerations correspond to the overall laser parameter $\alpha_{\rm L} = 11.5$ nm with the laser intensity $I = 28$ kW/cm^2.

In principle, under the intense field, scatterings of electrons with lattice may lead to an enhancement of lattice heating and even lattice expansion. This will affect the properties of electronic transport [84,85] (though not the focus of this work), whereas here we consider the laser intensity with an appropriate order of ~10^4 W/cm^2, which is readily achievable and widely adopted in experiments [86–93] and is far below the usual intense laser fields of about 10^{13} W/cm^2 [94,95] until the even larger intensity of 10^{20} W/cm^2 [96]. And, due to the absence of photon absorption (see Sec. II A 1), one can potentially quench the thermal effect. On the other hand, the increase in lattice temperature may result in an escalation of phonon energy and in turn affect phonon-assisted intersubband transitions [97–99]. By virtue of the nonresonant laser fields we employed, the increase in electron temperature caused by absorption can be largely quenched, which clearly also suppresses the phonon-involved interband transitions.

IV. RESULTS AND DISCUSSION

Below we discuss the gate assisted optical multisubband SO control. To proceed, we first show our self-consistent solutions, which are helpful for elucidating the general features of SO control. Then, we emphasize the effects of the two (axial and transverse) components of tilted IHFL fields on the potential energy and the DOS of 2DEGs. Also, we discuss the dependence of SO coupling on these two components. Further, we dig into the cases of gate assisted TLF multisubband SO control in either relatively narrow or wide well, with the well width of 13 and 26 nm, respectively. Three realistic but distinct scenarios for the impact of intersubband SO terms on the spin-resolved multisubband energy dispersions are also discussed, featuring band crossing and avoided crossing with and without vertex corrections of the spin texture.

A. Self-consistent outcome

In Figs. 1(c)–1(e), we show the total self-consistent potential $V_{\rm sc}$ and wave functions ψ_ν ($\nu = 1, 2$) of the two subbands for the 13-nm well at $V_{\rm g} = -0.1$ eV, with the laser tilt angle $\theta = \pi/16$, $\pi/3$, and $2\pi/5$, respectively. For highlighting the laser-dressing effect, the self-consistent potential without laser field (without both laser and gate fields) is also shown alongside by the red (black) dotted curve. Before discussing our self-consistent outcome in detail, we first examine the features from the point of view of symmetry analysis. Clearly, the gate field triggers the SIA of the system so that the left and right sides of the well are not symmetric with respect to the well center [cf. black and red (dotted) curves]. This is crucial for the Rashba SO coupling, which directly depends on the SIA. Remarkably, the laser field, to a certain extent, tends to balance the SIA induced by $V_{\rm g}$ [cf. solid and dotted (red) curves]. The balanced SIA can also be reflected by the spatial distributions of the two-subband wave functions (ψ_1 and ψ_2), which are basically equally distributed in the left and right sides of the well at $\theta = 2\pi/5$ [Fig. 1(e)].

The laser-dressing effect on the confining potential and the electron wave functions is mainly dominated by the axial component (A_z or α_z) of laser field. Specifically, under the impact of the laser-dressing effect, the laser axial component greatly alters the *effective* width of the well and so the potential profile [Figs. 1(c)–1(e)]. There exist two distinct regimes for the laser-dressed potential as the tilt angle θ varies, marked off around $\theta = \pi/3$ (corresponding to $\alpha_z \sim L_{\rm w}/2 = 6.5$ nm), in the parameter range considered. In the first regime, where θ is relatively large and greater than $\pi/3$, so that the axial laser parameter α_z is less than $L_{\rm w}/2$ (half of the well width), the laser field is apt to shrink the width of the lower half of the well, while tends to widen the upper half of the well [cf. dotted and solid (red) curves in Fig. 1(e)]. And, this feature becomes more pronounced as θ decreases (i.e., α_z increases), and consequently the well potential eventually exhibits a triangular profile when $\theta = \pi/3$, following from the laser-induced width quenching of the lower half of the well [Fig. 1(d)]. Remarkably, for even smaller tilt angle of $\theta < \pi/3$ (i.e., $\alpha_z > L_{\rm w}/2$), referring to the second regime of the laser-dressing effect, a transition from the original *single* well to an effective *double* well occurs [Fig. 1(c)]. In addition to effectively modifying the well width, the laser field also behaves as lowering the barrier height of the self-consistent potential $V_{\rm sc}$ seen by electrons [cf. dotted and solid (red) curves in Fig. 1(c)]. This arises from the dressing of the well confinement potential by the laser axial component and the modification of electron DOS (and so the electron Hartree potential) by the laser transverse component [100].

The above laser-dressing effect greatly alters the confinement potential energy with the change of the well width and the barrier height. This, together with the SIA induced by an external gate voltage, offers the feasibility of flexible SO control over both Rashba and Dresselhaus terms, which primarily depend on the gate bias and quantum confinement, respectively. To see the laser-dressing effect in a more direct manner, below we show how the axial component α_z of tilted laser field dresses the *structural* potential energy with $V_{\rm w} \to \widetilde{V}_{\rm w}$, i.e., in the absence of self-consistent procedure, and further describe how the laser transverse component α_x alters the DOS of 2DEGs.

B. Laser-dressed potential and laser-modified DOS

In Figs. 2(a)–2(c), we show the laser-dressed structural potential $\widetilde{V}_{\rm w}$ (i.e., without self-consistence) for the 13-nm well at $\alpha_z = 2$, 6.5, and 9 nm, respectively [see solid (red) curves]. The dotted (black) curve refers to the original

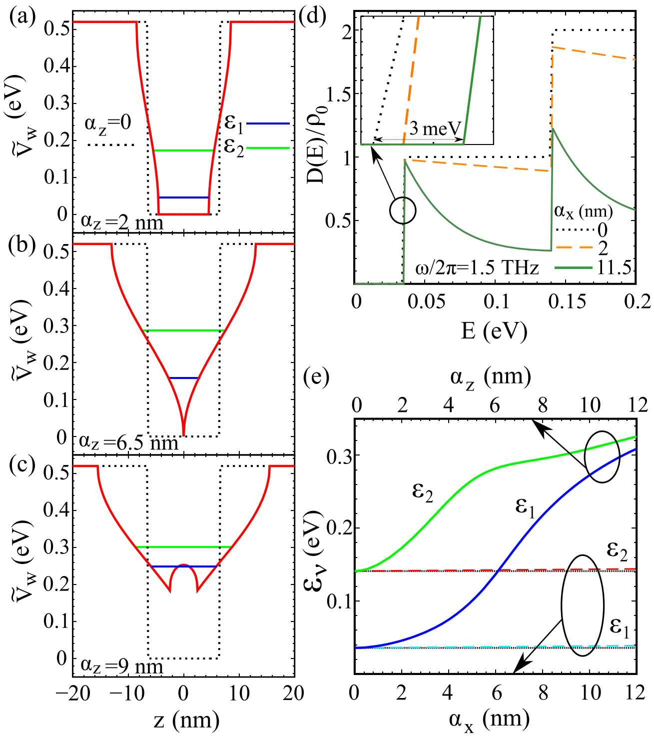

FIG. 2. [(a)–(c)] Laser-dressed structural potential ($\widetilde{V}_w$) of the 13-nm GaInAs well with only the TLF axial component being present ($\theta = 0$), at $\alpha_z = 2$ nm (a), 6.5 nm (b), 9 nm (c), indicating that the quantum well transits from the usual single well to an effective double well as the laser field strengthens. The dotted (black) curve representing the pure structural (square) potential (V_w), with $\widetilde{V}_w \to V_w$ when $\alpha_z \to 0$, is shown alongside, for highlighting the laser-*dressing* effect. The horizontal blue (green) line inside the well indicates the energy level $\mathcal{E}_1$ ($\mathcal{E}_2$) of the first (second) subband. (d) DOS of 2DEGs with only the transverse component of TLF being present ($\theta = \pi/2$), of the frequency $\omega/2\pi = 1.5$ THz, at $\alpha_x = 0$, 2, 11.5 nm. The inset shows a blowup of an *inconspicuous* energy blueshift of about 3 meV as α_x increases from 0 to 11.5 nm. (e) $\mathcal{E}_\nu$ ($\nu = 1, 2$) versus the axial (α_z; upper axis) and transverse (α_x; lower axis) laser parameters. The black dotted lines refer to the case of zero laser field (i.e., $\alpha_z = \alpha_x = 0$). In [(a)–(e)], the gate voltage is held at zero bias.

(undressed) structural potential V_w in the case of $\alpha_z = 0$. Here, we can more visibly see the two distinct regimes of the laser-dressing effect, indicating the transition of our system from a usual single well [Fig. 2(a) at $\alpha_z = 2$ nm] to an effective double well [Fig. 2(c) at $\alpha_z = 9$ nm], with intermediated potential featuring a triangular profile [Fig. 2(b) at $\alpha_z = L_w/2 = 6.5$ nm]. And, in the single-well regime of $\alpha_z < L_w/2$, the lower half of the well confinement (i.e., $\widetilde{V}_w < \delta_c/2 = 0.26$ eV) essentially shrank, while the upper half of the well confinement (i.e., $\widetilde{V}_w > \delta_c/2$) tends to be enlarged. When $\alpha_z > L_w/2$, referring to the double-well regime, the effective barrier height is greatly suppressed as compared to the undressed structural potential [cf. red (solid) and black (dotted) curves in Fig. 2(c)]. Clearly, the total self-consistent potential V_{sc} basically inherits all the features of the laser-dressing effect on the structural potential V_w [cf. Figs. 1(c)–1(e) and 2(a)–2(c)].

We should emphasize that, as α_z varies, the well width and the barrier height, both of which are the main sources affecting the quantum confinement of electrons, in general are simultaneously altered under the impact of laser field. This gives rise to a direct consequence that the electrons occupying the two subbands may *see* contrasting change of quantum confinement, in particular when the half of the barrier height is *sandwiched* between the energy levels of the two subbands, i.e., $\mathcal{E}_1 < \delta_c/2$ and $\mathcal{E}_2 > \delta_c/2$. In this configuration, clearly, the first- and second-subband electrons are locally subjected to a well which effectively becomes widened and narrowed, respectively. We will analyze these features in more detail later on for the optical response of the energy levels [Fig. 2(e)] and for the SO control.

Now we turn to the effect of the transverse component (α_x) of laser field on 2DEGs. Figure 2(d) shows the DOS dependence of 2DEGs on the energy at $\omega/2\pi = 1.5$ THz for several values of α_x, with $\alpha_x = 0$, 2, and 11.5 nm, corresponding to $F_x = 0$, 0.5, and 2.5 kV/cm, respectively. In contrast to the usual ladder profile of the 2D DOS at $\alpha_x = 0$ [dotted (black) curve], the laser transverse component tends to quench the DOS of 2DEGs. And, the reduction of the 2D DOS becomes more distinct with the enhancement of α_x [cf. dashed (orange) and solid (green) curves]. Note that the laser-modified DOS may vary the self-consistent electron Hartree potential V_e by altering the density of electrons, and consequently adjust the SO strengths (Sec. II C). In addition to modifying the DOS of 2DEGs, the transverse component also causes a slight energy blueshift of about 3 meV, as shown in the inset of Fig. 2(d). We should emphasize that this energy blueshift is independent of the subbands, namely, for either subband the blueshift is $\Delta E = 2\gamma\hbar\omega$, which depends on the laser strength of the transverse component through the parameter γ (see Sec. II A 2) and the laser oscillation frequency ω.

The laser-dressed potential and the laser-modified DOS will surely affect the quantized energy levels of 2DEGs. In Fig. 2(e), we show the energy levels $\mathcal{E}_1$ and $\mathcal{E}_2$ of the two subbands as functions of the laser axial component α_z (upper axis) and transverse component α_x (lower axis). We find that both $\mathcal{E}_1$ and $\mathcal{E}_2$ increase significantly as α_z grows. More specifically, for a lower value of α_z of less than 5 nm, both energy levels $\mathcal{E}_1$ and $\mathcal{E}_2$ are below $\delta_c/2$, and the quantum confinement for electrons of both subbands intensifies due to shrinking of the effective well width as α_z increases. Clearly, with the increasing of α_z, the second-subband energy level will eventually rise above $\delta_c/2$, and accordingly the electrons occupying the second subband will effectively *see* a widening well. In this situation, clearly, the two-subband electrons see contrasting quantum confinement, thus allowing for distinct SO control for electrons of the two subbands. On the other hand, in contrast to the strong energy dependence of $\mathcal{E}_\nu$ on α_z, it is found that both $\mathcal{E}_1$ and $\mathcal{E}_2$ depend very weakly on α_x, with a blueshift of only about 3 meV [see also the inset of Fig. 2(d)].

The above features of the laser-dressed potential and laser-modified DOS suggest that the two components of laser polarization are expected to manipulate SO terms from contrasting perspectives, both of which (from distinct physical sources) potentially have direct impacts on SO control. These results are helpful for understanding the underlying physics of

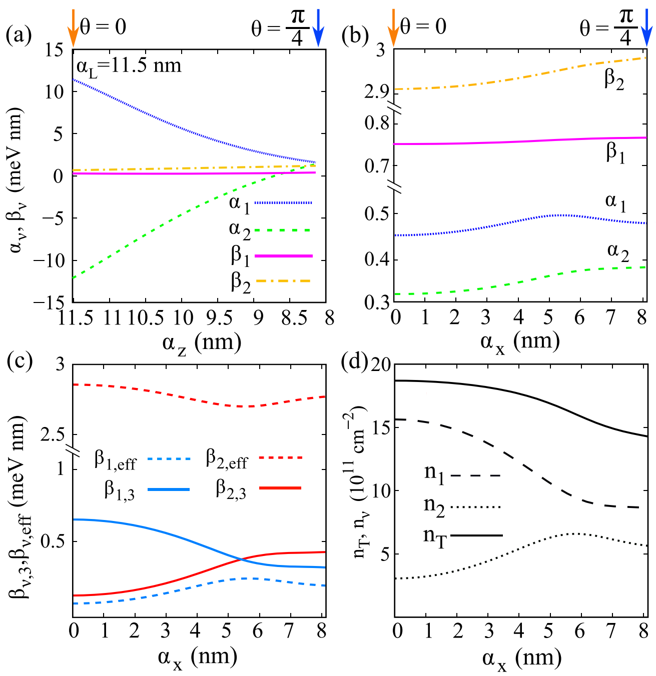

FIG. 3. (a), (b) The Rashba α_ν and the linear Dresselhaus β_ν ($\nu = 1, 2$) coefficients for the 13-nm GaInAs well, as functions of the TLF axial component α_z (a) and of the TLF transverse component α_x (b), when the tilt angle θ ranges from 0 to $\pi/4$, as indicated by the orange and blue (downward) arrows. (c) Dependence of the cubic ($\beta_{\nu,3}$) and the renormalized ($\beta_{\nu,\mathrm{eff}} = \beta_\nu - \beta_{\nu,3}$) Dresselhaus coefficients on α_x. (d) Subband occupations n_ν of 2DEGs versus α_x, with the total 2D electron density $n_T = n_1 + n_2$. For highlighting distinct and individual SO control of the two TLF components (α_z and α_x), in (a), $\alpha_z = \alpha_\mathrm{L}\cos\theta$, while we set $\alpha_x = 0$ (instead of $\alpha_x = \alpha_\mathrm{L}\sin\theta$); similarly, in (b)–(d), $\alpha_x = \alpha_\mathrm{L}\sin\theta$, while we consider $\alpha_z = 0$. The gate potential is chosen as $V_\mathrm{g} = -0.1$ eV, and the overall laser parameter is set at $\alpha_\mathrm{L} = 11.5$ nm.

the gate assisted optical multisubband SO control in quantum wells subjected to tilted laser fields. Below we first analyze the SO manipulation by solely the axial and transverse components of the laser polarization, respectively, and then discuss the *intertwined* effect of the two components on the spin-related properties.

C. SO control by two components of TLF

To unveil distinct and individual SO manipulation by the two components of TLF, we first look into the effect of the axial component on the control of SO coupling. Figure 3(a) shows the Rashba and Dresselhaus strengths for the 13-nm well at the gate potential $V_\mathrm{g} = -0.1$ eV, as functions of the axial laser parameter α_z ($= \alpha_L \cos\theta$) when the tilt angle varies from 0 to $\pi/4$. Note that the overall laser parameter is held fixed at $\alpha_\mathrm{L} = 11.5$ nm, corresponding to α_z ranging from 11.5 to 8.2 nm, which is greater than $L_w/2$. This indicates that the system is in the regime of an effective double well [Sec. IV B; Fig. 2(c)], due to the dressing effect of the axial component of laser polarization. Also, we should emphasize that, to only highlight the effect of axial component α_z on the SO control, we have set in Fig. 3(a) $\alpha_x = 0$ instead of $\alpha_x = \alpha_\mathrm{L}\sin\theta$.

For the Rashba couplings of the two subbands, we reveal that α_1 and α_2 essentially have the same strength, i.e., $|\alpha_1| = |\alpha_2|$. As α_z varies from 11.5 to 8.2 nm, the system features a double-well profile, and thus the electrons occupying the first and second subbands are mainly residing in the right and left subwells [Fig. 1(c)], respectively. In the double-well regime, the dressing effect may to a certain extent balance the relative gate-induced SIA seen by electrons of the two subbands in the two subwells, thus resulting in the Rashba coefficients α_1 and α_2 of essentially equal strength in magnitude. Further, we find that α_1 and α_2 also have opposite signs, and thus the relation $\alpha_1 \approx -\alpha_2$ holds. Note that the matching condition of two-subband Rashba terms is achieved in essentially the whole range of α_z considered [Fig. 3(a)], not at a specific value of α_z, greatly facilitating the formation of the so-called persistent skyrmion lattice that we recently proposed [17], which embraces *crossed* features of two spin helices. Contrasting signs of α_1 and α_2 arise from opposite direction of the force field [i.e., the derivative of potential energy in Eq. (20)] exerting on electrons of the two subbands, corresponding to the flip of SIA between the right and left subwells [38,40,43,61], which mostly host the first- and second-subband electrons, respectively. Moreover, both α_1 and α_2 decrease in their strength as α_z decreases. This is mainly attributed to the fact that the weakening of α_z alleviates the local SIA seen by electrons of the two subbands, and further leads to essentially the symmetric distribution of two-subband wave functions [Sec. IV A; Fig. 1(e)].

We should emphasize that all the above features of the dependence of Rashba coeffcients on α_z dominate the synchronous symmetric multisubband SO control that we will emphasize later on in Sec. IV D. Regarding the Dresselhaus terms β_1 and β_2, we observe that they basically remain inertia to α_z since the quantum confinement is only slightly altered with the reduction of α_z in the regime of an effective double well induced by the laser-dressing effect.

Now we have a look at the control of the Rashba and Dresselhaus couplings solely by the laser transverse component α_x, as shown in Fig. 3(b). The transverse component, which primarily affects the DOS of 2DEGs, clearly alters our self-consistent solutions (energy levels and wave functions) and so the relevant SO terms (Sec. II C). Despite this, for the GaInAs wells considered here, we observe that the Rashba α_ν and linear Dresselhaus β_ν SO coefficients for both subbands have relatively weak dependence on α_x. This is mainly because the DOS of 2DEGs modified by α_x has no direct consequence in affecting the SIA of the system and the quantum confinement, which are the key sources determining the Rashba α_ν and Dresselhaus β_ν strengths, respectively. To see the underlying physics in more detail, in the Supplemental Material (SM; Fig. S1) [101], we show all distinct ingredient contributions to the Rashba couplings of the two subbands for the 13-nm well, including the electron Hartree contribution α_ν^e, the gate plus doping contribution $\alpha_\nu^\mathrm{g+d}$, the pure structural contribution α_ν^w, and the laser field contribution α_ν^L. From Fig. S1 in the SM [101], we reveal that it is mainly the electron Hartree contribution α_ν^e dominating the dependence of the overall Rashba coupling $\alpha_\nu = \alpha_\nu^\mathrm{e} + \alpha_\nu^\mathrm{g+d} + \alpha_\nu^\mathrm{w} + \alpha_\nu^\mathrm{L}$ on the laser transverse component, following from that the change of DOS consequently alters the 3D electron density and so the electron

Hartree potential V_e, which directly determines α_ν^e (Sec. II C). In addition, the tunability of the Rashba term via the laser transverse component turns to become more distinct in even wider quantum wells, where the two-subband electrons have much broader spatial distributions (see Fig. S2 in the SM [101] for the well of width of $L_w = 26$ nm), which we will analyze in more detail later on in Sec. IV F for the laser tilt angle dependence of SO control.

On the other hand, even though the laser transverse component has no direct consequence on the linear Dresselhaus terms β_1 and β_2, it, however, can directly affect the 2D electron density n_T of the well [Fig. 3(d)], i.e., the electron occupations n_ν of the two subbands with $n_T = n_1 + n_2$, via the laser modified DOS of electrons, so it is expected to be more feasible to adjust the cubic $\beta_{\nu,3} = \gamma\pi n_\nu/2$ and renormalized $\beta_{\nu,\text{eff}} = \beta_\nu - \beta_{\nu,3}$, which are crucial for determining the correct symmetry points of the persistent spin helix [17,18,61]. The dependence of $\beta_{\nu,3}$ and $\beta_{\nu,\text{eff}}$ on α_x is shown in Fig. 3(c). We find that $\beta_{1,3}$ ($\beta_{2,3}$) largely decreases (increases) with increasing of α_x, directly following from the dependence of n_1 (n_2) on α_x [Fig. 3(d)]. And, the tunability of $\beta_{\nu,\text{eff}}$, which exhibits opposite dependence on α_x to $\beta_{\nu,3}$, alongside the control of the corresponding Rashba terms of distinct subbands, is in favor of the formation of multisubband persistent spin helices [17,38], for which the compensated SO strengths of Rashba and renormalized Dresselhaus terms for both subbands need to be simultaneously satisfied, i.e., $\alpha_1 = \pm\beta_{1,\text{eff}}$ and $\alpha_2 = \pm\beta_{2,\text{eff}}$.

D. Synchronous symmetric control of the two-subband Rashba couplings

Having the knowledge of the individual SO control by respectively the axial and transverse components of polarization for tilted laser field, now we are ready to analyze how to engineer the Rashba and Dresselhaus SO couplings by resorting to the geometrical tilt angle θ of laser field having both of the two polarization components.

Figure 4(a) shows the Rashba α_ν and Dresselhaus β_ν strengths of the two subbands as functions of θ for the 13-nm well at $V_g = 0$. Due to the lack of SIA of the well at zero gate bias, the Rashba coefficiets of the two subbands identically vanish for all angles of $\theta \in [0, \pi/2]$ [blue and green curves in Fig. 4(a)]. In contrast, for the Dresselhaus term [pink and yellow curves in Fig. 4(a)], first, we observe that β_1 and β_2 change very slightly when θ varies from 0 to $\pi/4$, primarily due to the axial component α_z, under which the well is in the regime of an effective double well, similar to that in Fig. 3(a). However, as θ further increases, the double-well profile will eventually turn into an effective triangular one around $\theta \sim \pi/3$. In this case, the quantum confinement effect is significantly enhanced with the reduction of α_z as θ increases, resulting in considerable increment of β_1 and β_2. Furthermore, when $\theta > \pi/3$, the well will be restored to the original single-well profile. Thus, further reduction of the axial component, one the one hand, leads to the widening of the lower half of the well, while on the other hand, results in the increasing of barrier height [Fig. 2(a)]. Clearly, the broadening of well width and the increasing of barrier height have opposite consequences on the quantum confinement.

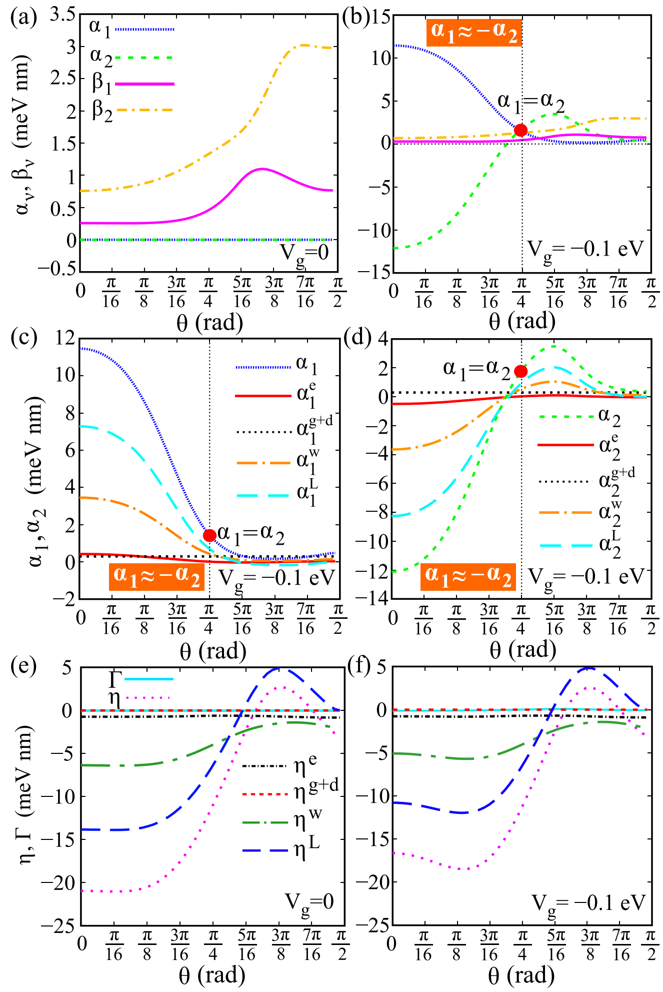

FIG. 4. (a), (b) Intrasubband Rashba α_ν and Dresselhaus β_ν ($\nu = 1, 2$) coefficients of the two subbands as functions of the TLF tilt angle θ, for the 13-nm GaInAs well at $V_g = 0$ (a) and $V_g = -0.1$ eV (b). (c), (d) Several distinct constituent contributions to the Rashba terms α_1 (c) and α_2 (d) versus θ for the well at $V_g = -0.1$ eV, including the electron Hartree contribution α_ν^e, the gate plus doping contribution α_ν^{g+d}, the pure structural contribution α_ν^w, and the laser field contribution α_ν^L. In [(b)–(d)], the vertical (black; dotted) line at $\theta \sim \pi/4$ marks $\alpha_1 = \alpha_2$ (indicated also by the red solid dot). In (c) and (d), the relation $\alpha_1 \approx -\alpha_2$ largely holds as θ varies when $\theta < \pi/4$. (e), (f) Dependence of the intersubband Rashba η and Dresselhaus Γ coefficients on θ for the well at $V_g = 0$ (e) and -0.1 eV (f). In (e) and (f), similar to $\alpha_\nu^{j=e,g+d,w,L}$, several different ingredient contributions η^j to η are also shown. The overall laser parameter is set at $\alpha_L = 11.5$ nm.

Since the energy level of the first subband $\mathcal{E}_1$ is mostly below the the critical value of $\delta_c/2 = 0.26$ eV in the parameter range considered [Fig. 2(e)], depending on the second-subband energy level $\mathcal{E}_2$ being below or above $\delta_c/2$, β_1 and β_2 may behave contrasting dependence on the tilt angle θ (cf. β_1 and β_2).

When the gate bias is switched on, the SIA of the well is induced, giving rise to finite Rashba SO couplings. In Fig. 4(b), we show both Rashba and Dresselhaus SO coefficients as functions of θ for the 13-nm well at $V_g = -0.1$ eV. For the optical response of Rashba terms, in a certain range of tilt angle $\theta \in [0, \pi/4]$ [to the left of the vertical dotted (black) line], we find that α_1 and α_2 exhibit similar laser dependence with essentially the same magnitude but opposite signs, i.e., $\alpha_1 \approx -\alpha_2$. This arises from the mitigation of the local SIA seen by electrons of the two subbands in the aforementioned double-well regime, as a result of the combined contributions from the laser-dressing effect of α_z [see also Figs. 2(c) and 3(a)] and the modification of α_x on electron Hartree potential through the adjustment of 2D electron density. The symmetric Rashba control of α_1 and α_2 via the geometric angle θ, provides a *synchronous* manipulation of the two-subband Rashba SO couplings over a wide range of laser polarizations, rather than being restricted to a unique value, greatly facilitating the realization of persistent skyrmion lattice that we recently proposed [17], even with different pitches. On the other hand, when θ is greater than $\pi/4$ [to the right of the vertical dotted (black) line], as θ varies we reveal that α_1 and α_2 could have the same sign, or even α_1 vanishes while α_2 is finite, greatly facilitating selective SO manipulation of distinct subbands. Note that, the vanishing Rashba coupling of the first subband is related to a *seemingly* symmetric configuration *seen* locally by the electrons occupying the first subband [Fig. 1(d)]. This provides a means for selectively suppressing the SO-induced spin relaxation mechanisms among distinct subbands. In contrast, for the laser dependence of Dresselhaus coefficients, we find that the changes of β_1 and β_2 in Fig. 4(b) are essentially consistent with that in Fig. 4(a), indicating that the linear Dresselhaus terms are not sensitive to electric control. Note that, in the parameter range considered, we reveal that the laser tunability of Rashba terms are much more distinct than that of Dresselhaus terms.

To further explore the underlying physics of the gate-assisted TLF control of the Rashba couplings, in Figs. 4(c) and 4(d), we show α_ν of the two subbands and the corresponding constituent contributions $\alpha_\nu^{\mathrm{e,g+d,w,L}}$ as functions of θ for the 13-nm well at $V_{\mathrm{g}} = -0.1$ eV. For the gate plus doping contribution $\alpha_\nu^{\mathrm{g+d}}$, it is found that $\alpha_1^{\mathrm{g+d}} = \alpha_2^{\mathrm{g+d}}$, which is attributed to a constant force field of $F_{\mathrm{g+d}} = -dV_{\mathrm{g+d}}/dz$ since the potential $V_{\mathrm{g+d}}$ is linear across the whole 2DEG region [18,37,43]. Regarding the electron Hartree contributions α_ν^{e}, as the electrons of the first and second subbands tend to reside on opposite sides of the well [61], the force field $F_{\mathrm{e}} = -dV_{\mathrm{e}}/dz$ for the two subbands largely has opposite signs, thus resulting in α_1^{e} and α_2^{e} essentially being opposite in their signs. As for the structural α_ν^{w} and laser field α_ν^{L} contributions, we observe that α_1^{w} (α_1^{L}) and α_2^{w} (α_2^{L}) almost have the same magnitude but opposite signs, and dominate over $\alpha_\nu^{\mathrm{g+d}}$ and α_ν^{e} in magnitude. Thus, here we attribute α_ν^{w} and α_ν^{L} to the main ingredient contributions to the synchronous symmetric control of the two-subband Rashba SO couplings.

E. Intersubband Rashba and Dresselhaus couplings

Figure 4(e) shows the intersubband Rashba term η including its constituent contributions $\eta^{\mathrm{e,g+d,w,L}}$ and the Dresselhaus term Γ as functions of the laser tilt angle θ, for the 13-nm well at zero gate bias. Due to different parities of the wave functions ψ_1 and ψ_2 of the two subbands, the intersubband Dresselhaus strength Γ in quantum wells without SIA maintains zero, regardless of which direction the laser polarization aligns in, as is expected [17]. In contrast, the intersubband Rashba coefficient η, which mainly depends on the overlap of the two-subband wave functions, has distinct dependence on θ and even features a sign reversal as θ varies. Regarding the constituent contributions of η, we find that the gate plus doping contribution $\eta^{\mathrm{g+d}}$ is identically zero, following from (i) the orthogonality condition for ψ_1 and ψ_2 of the two subbands and (ii) the gate plus doping potential $V_{\mathrm{g+d}}$ being linear across the well region hosting 2DEGs [18,37,43]. And, the electron Hartree contribution η^{e}, which mainly depends on the electron density, also exhibits inertia as θ varies. As a consequence, similar to the intrasubband Rashba term α_ν, the intersubband Rashba term is also mainly determined by the structural η^{w} and laser field η^{L} contributions.

Even the gate voltage is switched on with the emergence of SIA of the well, we reveal similar features of the optical control of the intersubband SO couplings for both Rashba η and Dresselhaus Γ terms [cf. Fig. 4(e) at $V_{\mathrm{g}} = 0$ and Fig. 4(f) at $V_{\mathrm{g}} = -0.1$ eV]. Specifically, even in the presence of SIA, which is expected to alter the symmetry of the wave functions and to quench the spatial overlap between ψ_1 and ψ_2, the Dresselhaus term Γ still basically remains zero and the Rashba term η essentially has the same magnitude as that at zero gate bias [cf. Figs. 4(f) and 4(e)]. This is primarily because the laser field may compensate the SIA of the well induced by the electrical gate bias, as is aforementioned [Fig. 1(e)].

Note that the nonzero intersubband Rashba SO coupling may give rise to intriguing physical phenomena, e.g., unusual *Zitterbewegung* [103] as well as band crossing and anticrossings of multiband spin branches [38]. Further, the intersubband SO term has also been experimentally verified in 2D electron systems with, e.g., unusual spin textures [34] and intrinsic spin-Hall effect [35]. Flexible control of the intersubband terms via TLFs, alongside the intrasubband terms, may trigger more interesting SO effects and the corresponding spintronic applications.

F. Gate assisted optical SO control in a relatively wide well

For capturing the full scenario of the gate assisted optical multisubband SO control, in Fig. 5(a) we show the intrasubband Rashba and Dresselhaus SO coefficients as functions of θ in a relatively wide well of $L_{\mathrm{w}} = 26$ nm. Clearly, the quantum confinement in wide wells is greatly quenched, and accordingly the energy levels of the two subbands are both below the critical energy $\delta_c/2$. This directly follows that the linear Dresselhaus coefficients β_1 and β_2 of the two subbands, which are dominated by quantum confinement, are relatively small. Meanwhile, due to the compensating contributions of the laser-dressing effect on the effective well width and barrier height to the degree of quantum confinement, β_1 and β_2 are also weakly dependent on θ. As for the intrasubband Rashba coefficients, remarkably, we also achieve adjusting the two Rashba terms in a selective manner with large flexibility. Specifically, as TLF varies, we manage to pin the first subband α_1 at zero, as indicated by the shadowed region in Fig. 5(a), while meanwhile to flexibly alter the second subband α_2, i.e., $\{\alpha_1 = 0, \alpha_2 \neq 0\}$. These features are in stark contrast to the aforementioned synchronous symmetric control of α_1 and α_2,

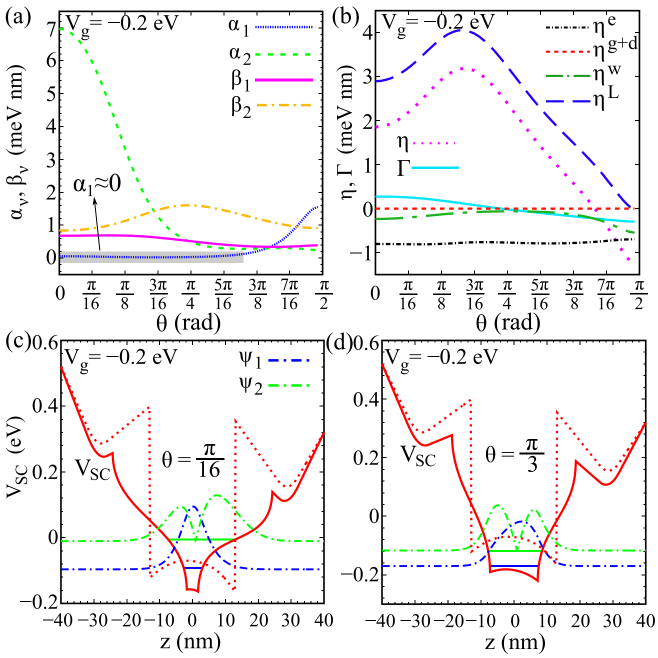

FIG. 5. (a) Intrasubband Rashba α_ν and Dresselhaus β_ν ($\nu = 1, 2$) coefficients of the two subbands as functions of the TLF tilt angle for the 26-nm GaInAs well. The shadowed region indicates that the Rashba term α_1 of the first subband essentially vanishes when $\theta < 3\pi/8$. (b) Dependence of the intersubband Rashba η and Dresselhaus Γ terms on θ, including several constituent contributions to η: the electron Hartree η^e, the gate plus doping η^{g+d}, the pure structural η^w, and the laser field η^L contributions. (c), (d) Self-consistent potential V_{sc} and wave functions ψ_ν for the 26-nm well at $\theta = \pi/16$ (c) and $\pi/3$ (d), with the dotted (red) curve referring to V_{sc} without TLF. The horizontal blue (green) line inside the well indicates the self-consistent energy level $\mathcal{E}_1$ ($\mathcal{E}_2$) of the first (second) subband. The gate potential is set at $V_g = -0.2$ eV and the overall laser parameter is chosen as $\alpha_L = 11.5$ nm.

which have opposite signs while are essentially locked to the same magnitude as θ varies, for the relatively narrow well of $L_w = 13$ nm. We should emphasize that here the consistent pinning of α_1 at zero within a large range of laser polarization, to a large extent, facilitates the suppression of electron spin relaxation for a given subband, while meanwhile allows for SO control of another subband in great flexibility, greatly fascinating for selective SO control in spintronic applications. Recently, we also achieved a similar selective Rashba control of distinct subbands, but with $\{\alpha_1 \neq 0, \alpha_2 = 0\}$ and under the stringency of a specific value of gate voltage or laser parameter [32,43]. This together with the TLF-mediated wide-range selective SO control of $\{\alpha_1 = 0, \alpha_2 \neq 0\}$ opens more possibilities for practical applications in which a full scenario of selective SO control is important.

Now we analyze more in detail the TLF control of the two-subband Rashba couplings via the geometrical tilt angle. The vanishing of the first-subband Rashba term α_1 in Fig. 5(a) is due to the fact that the electrons occupying the first subband *see* a locally symmetric configuration, as a result of the balanced effect of the laser field on the SIA induced by the external gate bias. And, the local symmetric configuration seen by the first-subband electrons can also be reflected by the spatial distribution of the wave function ψ_1, which is symmetric with respect to the center of the well [see Fig. 5(c)]. While for the second subband, as θ increases, electrons are inclined to move from the right side of the well to the left side [cf. green curves (ψ_2) in Figs. 5(c) and 5(d)]. This process of charge transfer between left and right sides of the well quenches the SIA induced by gate field so that the force field seen by the second-subband electrons is shrinking, and accordingly leads to the reduction of the second-subband Rashba term α_2.

In addition to the intrasubband SO terms emphasized above, Fig. 5(b) shows the intersubband Rashba (including its constituent contributions) and Dresselhaus SO coefficients as functions of θ for the 26-nm well. Regarding the intersubband Dresselhaus term Γ, in contrast to that in the case of the 13-nm (relatively narrow) well, here it becomes finite and is readily tunable by the tilt angle θ. Notably, with the variation of θ, we find that Γ disappears at about $\theta = \pi/4$ and the sign of it can even be reversed as θ further increases. Despite this, we should emphasize that Γ is still much weaker than the intersubband Rashba term η that we will discuss next.

Regarding the intersubband Rashba term η, in addition to its much larger magnitude than Γ, we find that η can also change its sign as θ varies. This feature is similar to that for the 13-nm well, even though η is largely positive for the 26-nm well while is mostly negative for the 13-nm well, in the range of parameters considered [cf. Figs. 4(f) and 5(b)]. Furthermore, we note that here for the 26-nm well the laser field plays a very important role in η, for which the laser field contribution η^L almost dominates over all the other contributions of η^e, η^{g+d}, and η^w, indicating potential applications of flexible control of the intersubband SO terms via optical manner.

G. Combined control of the Rashba coupling via gate and TLF

Since the Dresselhaus SO coupling, which depends on quantum confinement, is mainly dominated by the laser field and in general is not sensitive to electric manipulation, here we mainly focus on the Rashba SO coupling of both relatively narrow (13-nm) and wide (26-nm) wells, for the combined control via the electrical gate bias and the tilted laser field. To this end, in Figs. 6(a) and 6(b), we show the grayscale map of the intrasubband Rashba terms α_1 (first subband) and α_2 (second subband), respectively, as functions of V_g and θ, for the 13-nm well. Note that several constant values of α_1 and α_2 are also shown by the contour lines with different colors. Clearly, within the range of $\theta \in [0, \pi/4]$, α_1 and α_2 have opposite signs and are essentially locked to equal strength, i.e., $\alpha_1 \approx -\alpha_2$, independent of the gate voltage, referring to the synchronized symmetric control of the Rashba terms of distinct subbands. Note that, under the combined action of the axial and transverse components of laser polarization, since α_1 and α_2 are locked to each other over a wide range of laser fields, this greatly facilitates the formation of multisubband persistent spin helices simultaneously [17].

Figures 6(c) and 6(d) show the Rashba coefficients of the two subbands for the relatively wide well of $L_w = 26$ nm. Clearly, α_1 is basically vanishing in most of the range of V_g and θ considered, due to the fact that the electrons of the

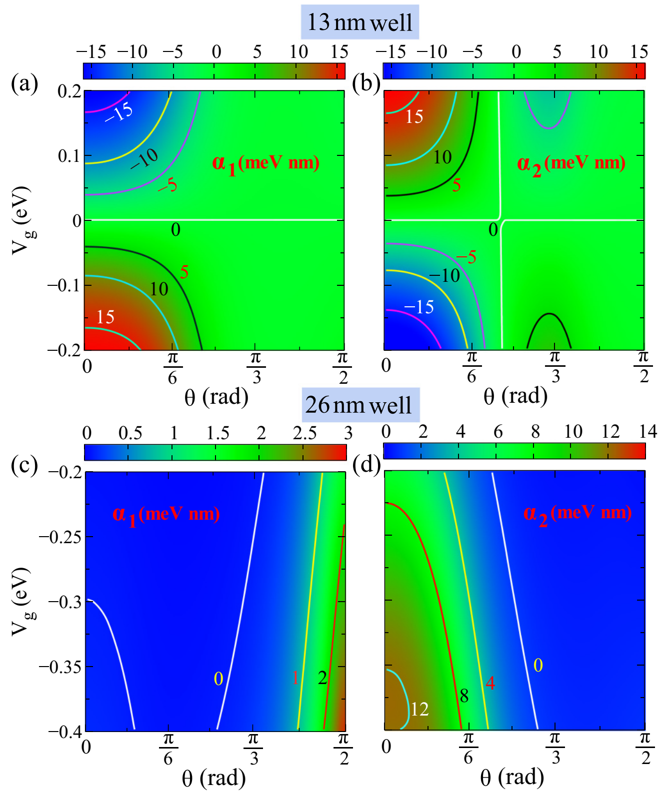

FIG. 6. (a), (b) Intrasubband Rashba coefficients α_1 (a) and α_2 (b) of the two subbands for the 13-nm GaInAs well, as functions of the gate voltage V_g and the TLF tilt angle θ. (c), (d) Refer to the corresponding analogs to (a) and (b), respectively, while for the 26-nm well. In [(a)–(d)], several values of contour lines of α_1 or α_2 are also shown. The overall laser parameter is set at $\alpha_L = 11.5$ nm.

first subband see approximately symmetric confining potential dressed by the laser field. And, because of the quenching of the effective force field as θ increases, α_2 also drops sharply to zero with θ. As a remark, the extensive electro-optical control of multisubband SO couplings via both external gate bias and tilted laser field greatly alleviates the strictness for the SO manipulation with solely the electrical means, highly desirable for practical applications.

H. Two types of avoided crossings with distinct spin textures: With and without vertex corrections

So far, we have separately discussed the intrasubband and intersubband SO terms in the presence of gate and laser fields. The flexible electro-optical control of the intrasubband and intersubband SO couplings inspires us to further explore the combined effect of them on the band dispersion and the spin texture, which are crucial for various corresponding spintronic applications, e.g., spin-charge conversion [104, 105]. As we emphasized above, by adjusting the gate and laser fields, the intrasubband Rashba terms α_1 and α_2 of the two subbands can have either the same or opposite signs, or even both α_1 and α_2 vanish (symmetric well) so that the only surviving intrasubband SO terms are the Dresselhaus types β_1 and β_2 (see Figs. 4 and 6). Therefore, without lack of generality, below we mainly focus on these three typical scenarios, i.e., (i) $\alpha_1 = \alpha_2$ (same sign), (ii) $\alpha_1 = -\alpha_2$ (opposite signs), and (iii) $\beta_1 = \beta_2$ ($\alpha_1 = 0, \alpha_2 = 0$). For the intersubband SO terms, below we only take into account the Rashba coupling η, as the Dresselhaus coupling Γ is much smaller than η in the parameter range considered [see Figs. 4(f) and 5(b)].

In Figs. 7(a)–7(c), we show the spin-resolved energy dispersions for the four spin branches (two for each subband) of the two subbands, for the above three scenarios (i)–(iii), respectively, under the impact of the intersubband Rashba term η. The dotted black curves are for the uncoupled case between the two subbands with $\eta = 0$ (i.e., without intersubband term), featuring the crossing of the spin branches of the two subbands.

Under the impact of the intersubband SO coupling η, we reveal that the four spin branches of the two subbands may maintain crossing [scenario (i); see green circle in Fig. 7(a)] or turn to avoided crossing [scenario (ii); see green circle in Fig. 7(b)], depending on the relative sign of the intrasubband terms α_1 and α_2, as compared to the uncoupled ($\eta = 0$) case. For both cases of crossing and avoided crossing, the usual Rashba chiral spin texture remains unchanged, i.e., the spin hybridization is not allowed [see size (the degree of spin polarization) and color (the spin direction) of markers in Figs. 7(a) and 7(b)]. However, in scenario (iii) when there are only Dresselhaus terms for the intrasubband SO coupling, referring to the case of the quantum well in the absence of SIA (e.g., $V_g = 0$), we unveil distinct spin textures with vertex corrections to the usual Rashba kinds, even though the energy dispersion itself is the same as that for scenario (ii) [cf. Figs. 7(b) and 7(c)]. Notably, near the avoided crossing, there is even vanishing spin polarization due to the hybridization of different spin branches. This is in stark contrast to the scenario (ii), where the avoided crossing of the energy dispersion essentially does not destroy the original spin texture in the absence of intersubband SO coupling, namely, without vertex corrections.

We should emphasize that the avoided crossing induced by the intersubband SO term has been experimentally verified in the Rashba surface states of Bi/Ag(111) and Bi/Cu(111) even with hybridized spin textures [34,106], where there exist physical phenomena related to the orbital mixing as well as the SO entanglement. These vertex corrections to the spin texture due to the interband terms may also lead to intriguing possibilities for spintronic applications, e.g., high-efficiency spin-charge conversion devices and the intrinsic spin-Hall effect [35,104,107].

V. CONCLUDING REMARKS

The intense and high-frequency laser field dresses the quantum confinement and alters the quantized energy levels in quantum confined systems, giving rise to intriguing control of electronic and optical properties of 2DEGs. Recently, we proposed the concept of *laser-dressing-effect* mediated SO control in semiconductor wells, with the laser polarization aligning with the well-growth direction [43], facilitating flexible SO control. Here, by resorting to TLFs with the interplay of laser axial and transverse components, we go much beyond that in Ref. [43], not only from the generic and comprehensive theoretical model itself (and practical applications)

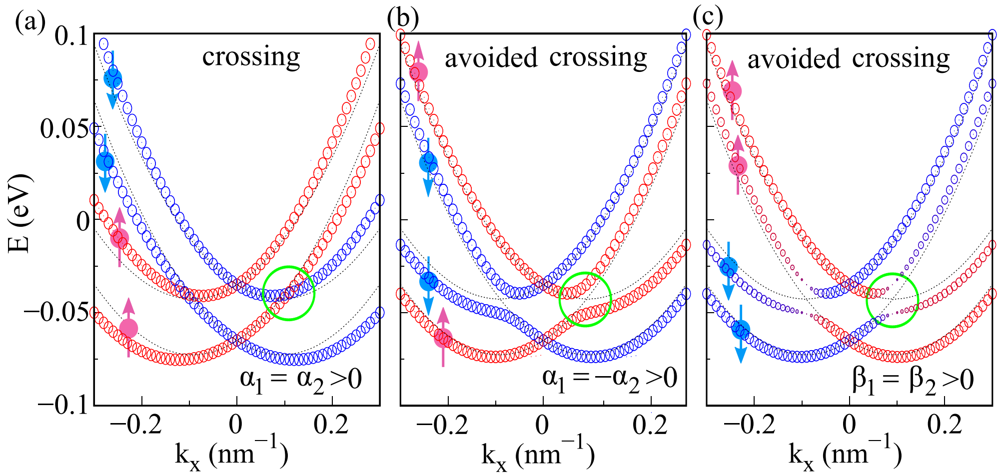

FIG. 7. Spin-resolved energy dispersions (scaled by a factor of 15 for visibility) with both intrasubband and intersubband SO terms of the four spin branches versus k_x [$\parallel$ (100)] of the AlInAs/GaInAs well, for $\{\alpha_1 > 0, \alpha_2 > 0\}$ (a), $\{\alpha_1 > 0, \alpha_2 < 0\}$ (b), and $\{\beta_1 > 0, \beta_2 > 0\}$ (c). The size of the marker scales with the degree of spin polarization and the color represents the spin orientations up (red) and down (blue), as indicated by the up and down arrows. The black dotted curves correspond to the uncoupled ($\eta = 0$) bands which clearly have crossing (as indicated by green circle), and for $\eta \neq 0$ the bands maintain crossing (a), or exhibit avoided crossing (b), (c), depending on the combined effect of intrasubband and intersubband terms. The SO coefficients are chosen for the 13-nm well at $V_g = -0.1$ eV and $\theta = \pi/16$ [Figs. 4(b) and 4(f)], with $\alpha_1 = \alpha_2 = 11$ meV nm for (a), $\alpha_1 = -\alpha_2 = 11$ meV nm for (b), and $\beta_1 = \beta_2 = 11$ meV nm for (c), and $\eta = -17.5$ meV nm. Note that the intersubband Dresselhaus term Γ is negligibly small and hence is omitted [Figs. 4(e) and 4(f)].

incorporating both of the two laser components, but also from the emerging new SO features, greatly fascinating for spintronic applications.

The two laser components are found to manipulate SO terms from distinct physical sources, with the axial component primarily dressing the quantum well and the transverse component mainly altering the electron DOS. Under the impact of TLFs, we have achieved a *synchronous* symmetric Rashba control of distinct subbands, i.e., $\alpha_1 = -\alpha_2$, over a wide range of laser polarization, rather than being restricted to a unique value of laser field, which greatly facilitates the realization of persistent skyrmion lattice (even with different pitches) that we recently proposed [17]. Also, we achieve adjusting the two Rashba terms in a selective manner, where α_1 can be pinned at zero as TLF varies while meanwhile α_2 can be flexibly adjusted, greatly fascinating for selective multisubband SO control in particular with suppressed spin relaxation for a given subband. As for the intrasubband Dresselhaus coupling, we unveil the optical tunability of linear β_ν terms and even the dependence of cubic $\beta_{\nu,3}$ and renormalized $\beta_{\nu,\mathrm{eff}}$ terms on laser transverse component. Moreover, we demonstrate that the magnitude and sign of the intersubband Rashba coupling η can be significantly manipulated by TLFs, which together with the intrasubband terms triggers the band crossing and anticrossing of multiband spin branches with and without vertex corrections, which are important for spintrobic applications, e.g., spin-charge conversion [104,105]. Our work sheds light on experiments incorporating the TLF for a universal control of the Rashba-Dresselhaus SO terms of both intrasubband and intersubband kinds.

In addition, our generic model can also be potentially used to explore SO features in other quantum systems, in which the laser transverse component may possibly dominate the SO control. For instance, for the GaInAs *triple* wells with three occupied subbands [38], due to the occupation of much higher-energy subbands, the laser transverse component may significantly adjust the relative electron distributions among distinct subbands and so the relevant SO strengths. Moreover, the TLF-mediated optical SO control may inspire further theoretical studies in *wurtzite* quantum systems, e.g., wide-gap GaN/AlGaN quantum wells [30]. The wurtzite heterostructures with strong built-in (spontaneous and piezoelectric) electrical fields have the insensitive electrical control of the usual Rashba coupling, let alone the Dresselhaus coupling.

As a final remark, here we only consider nonresonant laser fields without photon absorption, while we believe that the SO-mediated linear (and nonlinear) spin-dependent optical properties as well as spin transport and dynamics with phonon (and even impurity) scatterings, in particular, due to the thermal effects in the near-resonance scenario may be highly interesting. More work is needed to explore these possibilities.

ACKNOWLEDGMENTS

We thank J. Cheng, H. Cao, and S. Xu for valuable discussions about thermal effects related to intense laser fields. This work was supported by the National Natural Science Foundation of China (Grants No. 12274256, No. 11874236, No. 12022413, No. 11674331, and No. 61674096), the Major Basic Program of Natural Science Foundation of Shandong Province (Grant No. ZR2021ZD01), the National Key R&D Program of China (Grant No. 2022YFA1403200), and the "Strategic Priority Research Program (B)" of the Chinese Academy of Sciences (Grant No. XDB33030100). W.L. acknowledges financial support from the Natural Science Foundation of Shandong Province (Grant No. ZR2021QA108).

[1] D. Awschalom, D. Loss, and N. Samarth, *Semiconductor Spintronics and Quantum Computation* (Springer, New York, 2002).

[2] I. Žutić, J. Fabian, and S. D. Sarma, Spintronics: Fundamentals and applications, Rev. Mod. Phys. **76**, 323 (2004).

[3] J. Fabian, A. Matos-Abiague, C. Ertler, P. Stano, and I. Žutić, Semiconductor Spintronics, Acta Phys. Slovaca **57**, 565 (2007).

[4] P. Chuang, S. Ho, L. W. Smith, F. Sfigakis, M. Pepper, C. Chen, J. Fan, J. P. Griffiths, I. Farrer, H. E. Beere, G. A. C. Jones, D. A. Ritchie, and T. Chen, All-electric all-semiconductor spin field-effect transistors, Nat. Nanotechnol. **10**, 35 (2015).

[5] H. C. Koo, J. H. Kwon, J. Eom, J. Chang, S. H. Han, and M. Johnson, Control of spin precession in a spin-injected field effect transistor, Science **325**, 1515 (2009).

[6] S. Datta and B. Das, Electronic analog of the electro-optic modulator, Appl. Phys. Lett. **56**, 665 (1990).

[7] J. Sinova, S. O. Valenzuela, J. Wunderlich, C. H. Back, and T. Jungwirth, Spin Hall effects, Rev. Mod. Phys. **87**, 1213 (2015).

[8] J. Wunderlich, B. Park, A. C. Irvine, L. P. Zârbo, E. Rozkotová, P. Nemec, V. Novák, J. Sinova, and T. Jungwirth, Spin Hall effect transistor, Science **330**, 1801 (2010).

[9] J. Sklenar, W. Zhang, M. B. Jungfleisch, W. J. Jiang, H. Saglam, J. E. Pearson, J. B. Ketterson, and A. Hoffmann, Perspective: Interface generation of spin-orbit torques, J. Appl. Phys. **120**, 180901 (2016).

[10] Y. C. Lau, D. Betto, K. Rode, J. M. D. Coey, and P. Stamenov, Spin–orbit torque switching without an external field using interlayer exchange coupling, Nat. Nanotechnol. **11**, 758 (2016).

[11] S. D. Ganichev, E. L. Ivchenko, V. V. Bel'kov, S. A. STarasenko, M. Sollinger, D. Weiss, W. Wegscheider, and W. Prettl, Spin-galvanic effect, Nature (London) **417**, 153 (2002).

[12] B. A. Bernevig, T. L. Hughes, and S. C. Zhang, Quantum spin Hall effect and topological phase transition in HgTe quantum wells, Science **314**, 1757 (2006).

[13] R. M. Lutchyn, J. D. Sau, and S. Das Sarma, Majorana fermions and a topological phase transition in semiconductor-superconductor heterostructures, Phys. Rev. Lett. **105**, 077001 (2010).

[14] Y. Oreg, Y. Refael and F. von Oppen, Helical liquids and majorana bound states in quantum wires, Phys. Rev. Lett. **105**, 177002 (2010).

[15] R. Song, P. Zhang, and N. Hao, Phase-manipulation-induced majorana mode and braiding realization in iron-based superconductor Fe(Te,Se), Phys. Rev. Lett. **128**, 016402 (2022).

[16] H. M. Weng, C. Fang, Z. Fang, B. A. Bernevig, and X. Dai, Weyl semimetal phase in noncentrosymmetric transition-metal monophosphides, Phys. Rev. X **5**, 011029 (2015).

[17] J. Y. Fu, P. H. Penteado, M. O. Hachiya, D. Loss, and J. C. Egues, Persistent skyrmion lattice of noninteracting electrons with spin-orbit coupling, Phys. Rev. Lett. **117**, 226401 (2016).

[18] F. Dettwiler, J. Y. Fu, S. Mack, P. J. Weigele, J. C. Egues, D. D. Awschalom, and D. M. Zumbühl, Stretchable persistent spin helices in GaAs quantum wells, Phys. Rev. X **7**, 031010 (2017).

[19] P. J. Weigele, D. C. Marinescu, F. Dettwiler, J. Y. Fu, S. Mack, J. C. Egues, D. D. Awschalom, and D. M. Zumbuhl, Symmetry breaking of the persistent spin helix in quantum transport, Phys. Rev. B **101**, 035414 (2020).

[20] N. Zhao, Y. H. Duan, H. Yang, X. Li, W. Liu, J. H. Zhao, S. X. Han, K. Shen, N. Hao, J. Y. Fu, and P. Zhang, Two copies of persistent spin helices with stretching pitch and compensating helicity, Phys. Rev. B **107**, 205407 (2023).

[21] Y. A. Bychkov and E. I. Rashba, Properties of a 2D electron gas with lifted spectral degeneracy, JETP Letters **39**, 78 (1984).

[22] G. Dresselhaus, Spin-orbit coupling effects in zinc blende structures, Phys. Rev. **100**, 580 (1955).

[23] J. D. Koralek, C. P. Weber, J. Orenstein, B. A. Bernevig, S.-C. Zhang, S. Mack, and D. D. Awschalom, Emergence of the persistent spin helix in semiconductor quantum wells, Nature (London) **458**, 610 (2009).

[24] G. Engels, J. Lange, T. Schäpers, and H. Lüth, Experimental and theoretical approach to spin splitting in modulation-doped $In_xGa_{(1-x)}As/InP$ quantum wells for $B \to 0$, Phys. Rev. B **55**, R1958 (1997).

[25] J. Nitta, T. Akazaki, H. Takayanagi, and T. Enoki, Gate control of spin-orbit interaction in an inverted $In_{0.53}Ga_{0.47}As/In_{0.52}Al_{0.48}As$, Phys. Rev. Lett. **78**, 1335 (1997).

[26] N. S. Averkiev, L. E. Golub, and M. Willander, Spin relaxation anisotropy in two-dimensional semiconductor systems, J. Phys.: Condens. Matter **14**, R271 (2002).

[27] N. S. Averkiev and L. E. Golub, Giant spin relaxation anisotropy in zinc-blende heterostructures, Phys. Rev. B **60**, 15582 (1999).

[28] D. Iizasa, A. Aoki, T. Saito, J. Nitta, G. Salis, and M. Kohda, Control of spin relaxation anisotropy by spin-orbit-coupled diffusive spin motion, Phys. Rev. B **103**, 024427 (2021).

[29] M. P. Walser, C. Reichl, W. Wegscheider, and G. Salis, Direct mapping of the formation of a persistent spin helix, Nat. Phys. **8**, 757 (2012).

[30] J. Y. Fu, P. H. Penteado, D. R. Candido, G. J. Ferreira, D. P. Pires, E. Bernardes, and J. C. Egues, Spin-orbit coupling in wurtzite heterostructures, Phys. Rev. B **101**, 134416 (2020).

[31] C.-M. Hu, J. Nitta, T. Akazaki, H. Takayanagai, J. Osaka, P. Pfeffer, and W. Zawadzki, Zero-field spin splitting in an inverted $In_{0.53}Ga_{0.47}As/In_{0.52}Al_{0.48}As$ heterostructure: Band nonparabolicity influence and the subband dependence, Phys. Rev. B **60**, 7736 (1999).

[32] Q. X. Wang, H. Yang, and J. Y. Fu, Selective asymmetric gate control of the Rashba spin-orbit coupling in GaInAs/AlInAs stepped wells, Phys. Rev. B **101**, 245403 (2020).

[33] C.-M. Hu, J. Nitta, T. Akazaki, H. Takayanagi, J. Osaka, P. Pfeffer, and W. Zawadzki, Observation of the zero-field spin splitting of the second subband in an inverted $In_{0.53}Ga_{0.47}As/In_{0.52}Al_{0.48}As$ heterostructure, Phys. E (Amsterdam) **6**, 767 (2000).

[34] H. Bentmann, S. Abdelouahed, M. Mulazzi, J. Henk, and F. Reinert, Direct observation of interband spin-orbit coupling in a two-dimensional electron system, Phys. Rev. Lett. **108**, 196801 (2012).

[35] F. G. G. Hernandez, L. M. Nunes, G. M. Gusev, and A. K. Bakarov, Observation of the intrinsic spin Hall effect in a two-dimensional electron gas, Phys. Rev. B **88**, 161305(R) (2013).

[36] E. A. de Andrada e Silva, G. C. La Rocca, and F. Bassani, Spin-orbit splitting of electronic states in semiconductor asymmetric quantum wells, Phys. Rev. B **55**, 16293 (1997).

[37] R. S. Calsaverini, E. Bernardes, J. C. Egues, and D. Loss, Intersubband-induced spin-orbit interaction in quantum wells, Phys. Rev. B **78**, 155313 (2008).
[38] W. Liu, H. Yang, and J. Y. Fu, Unusual spin-orbit control in AlInAs/GaInAs triple wells triggered by band crossing and anticrossing, Phys. Rev. B **104**, 165428 (2021).
[39] M. P. Walser, U. Siegenthaler, V. Lechner, D. Schuh, S. D. Ganichev, W. Wegscheider, and G. Salis, Dependence of the Dresselhaus spin-orbit interaction on the quantum well width, Phys. Rev. B **86**, 195309 (2012).
[40] H. Yang, Q. X. Wang, and J. Y. Fu, Interface involved Dresselhaus spin-orbit coupling in GaInAs/AlInAs heterostructures, Phys. Rev. B **104**, 125426 (2021).
[41] J.-M. Jancu, R. Scholz, E. A. de Andrada e Silva, and G. C. La Rocca, Atomistic spin-orbit coupling and $k \cdot p$ parameters in III-V semiconductors, Phys. Rev. B **72**, 193201 (2005).
[42] L. Cheng, L. M. Wei, H. X. Liang, Y. D. Yan, G. H. Cheng, M. Lv, T. Lin, T. T. Kang, G. L. Yu, J. H. Chu, Z. Y. Zhang, and C. G. Zeng, Optical manipulation of Rashba spin–orbit coupling at $SrTiO_3$-based oxide interfaces, Nano Lett. **17**, 6534 (2017).
[43] X. Li, W. Wang, N. Zhao, H. Yang, S. X. Han, W. Liu, H. L. Wang, F. Y. Qu, N. Hao, J. Y. Fu, and P. Zhang, Intense high-frequency laser-field control of spin-orbit coupling in GaInAs/AlInAs quantum wells: A laser dressing effect, Phys. Rev. B **106**, 155420 (2022).
[44] J. González-Vázquez, I. R. Sola, J. Santamaria, and V. S. Malinovsky, Quantum control of spin–orbit coupling by dynamic stark-shifts induced by laser fields, Chem. Phys. Lett. **431**, 231 (2006).
[45] B. Chatel, D. Bigourd, S. Weber, and B. Girard, Coherent control of spin–orbit precession with shaped laser pulses, J. Phys. B: At., Mol. Opt. Phys. **41**, 074023 (2008).
[46] L. Meier, G. Salis, I. Shorubalko, E. Gini, S. Schön, and K. Ensslin, Measurement of Rashba and Dresselhaus spin–orbit magnetic fields, Nat. Phys. **3**, 650 (2007).
[47] E. H. Ahmed, S. Ingram, T. Kirova, O. Salihoglu, J. Huennekens, J. Qi, Y. Guan, and A. M. Lyyra, Quantum control of the spin-orbit interaction using the Autler-Townes effect, Phys. Rev. Lett. **107**, 163601 (2011).
[48] M. Gavrila and J. Z. Kaminski, Free-free transitions in intense high-frequency laser fields, Phys. Rev. Lett. **52**, 613 (1984).
[49] C. Pellegrini, A. Marinelli, and S. Reiche, The physics of x-ray free-electron lasers, Rev. Mod. Phys. **88**, 015006 (2016).
[50] H. Zimmermann, S. Meise, A. Khujakulov, A. Magaña, A. Saenz, and U. Eichmann, Limit on excitation and stabilization of atoms in intense optical laser fields, Phys. Rev. Lett. **120**, 123202 (2018).
[51] M. Kübel, M. Spanner, Z. Dube, A. Y. Naumov, S. Chelkowski, A. D. Bandrauk, M. J. J. Vrakking, P. B. Corkum, D. M. Villeneuve, and A. Staudte, Probing multiphoton light-induced molecular potentials, Nat. Commun. **11**, 2596 (2020).
[52] R. G. Mani, J. H. Smet, K. von Klitzing, V. Narayanamurti, W. B. Johnson, and V. Umansky, Zero-resistance states induced by electromagnetic-wave excitation in GaAs/AlGaAs heterostructures, Nature (London) **420**, 646 (2002).
[53] W. A. Barletta, J. Bisognano, J. N. Corlett, P. Emma, Z. Huang, K. J. Kim, R. Lindberg, J. B. Murphy, G. R. Neil, D. C. Nguyen, C. Pellegrini, R. A. Rimmer, F. Sannibale, G. Stupakov, R. P. Walker, and A. A. Zholents, Free electron lasers: Present status and future challenges, Nucl. Instrum. Methods Phys. Res., Sect. A **618**, 69 (2010).
[54] S. Kim, J. Jin, Y. J. Kim, I. Y. Park, Y. Kim, and S. W. Kim, High-harmonic generation by resonant plasmon field enhancement, Nature (London) **453**, 757 (2008).
[55] N. G. Asmar, A. G. Markelz, E. G. Gwinn, J. Černe, M. S. Sherwin, K. L. Campman, P. F. Hopkins, and A. C. Gossard, Resonant-energy relaxation of terahertz-driven two-dimensional electron gases, Phys. Rev. B **51**, 18041 (1995).
[56] N. H. Tolk, R. G. Albridge, A. V. Barnes, B. M. Barnes, J. L. Davidson, V. D. Gordon, G. Margaritondo, J. T. McKinley, G. A. Mensing, and J. Sturmann, Free-electron laser wavelength-selective materials alteration and photoexcitation spectroscopy, Appl. Surf. Sci. **106**, 205 (1996).
[57] B. G. Enders, F. M. S. Lima, O. A. C. Nunes, A. L. A. Fonseca, D. A. Agrello, F. Y. Qu, E. F. Da Silva, and V. N. Freire, Electronic properties of a quasi-two-dimensional electron gas in semiconductor quantum wells under intense laser fields, Phys. Rev. B **70**, 035307 (2004).
[58] E. C. Niculescu and A. Radu, Laser-induced diamagnetic anisotropy of coaxial nanowires, Curr. Appl. Phys. **10**, 1354 (2010).
[59] E. C. Niculescu, L. M. Burileanu, A. Radu, and A. Lupaşcu, Anisotropic optical absorption in quantum well wires induced by high-frequency laser fields, J. Lumin. **131**, 1113 (2011).
[60] T. Koga, J. Nitta, T. Akazaki, and H. Takayanagi, Rashba spin-orbit coupling probed by the weak antilocalization analysis in InAlAs/InGaAs/InAlAs quantum wells as a function of quantum well asymmetry, Phys. Rev. Lett. **89**, 046801 (2002).
[61] J. Y. Fu and J. C. Egues, Spin-orbit interaction in GaAs wells: From one to two subbands, Phys. Rev. B **91**, 075408 (2015).
[62] W. C. Henneberger, Perturbation method for atoms in intense light beams, Phys. Rev. Lett. **21**, 838 (1968).
[63] C. K. Choi, W. C. Henneberger, and F. C. Sanders, Intensity-dependent ionization potentials for H and He in intense laser beams, Phys. Rev. A **9**, 1895 (1974).
[64] J. I. Gersten and M. H. Mittleman, The shift of atomic states by laser fields, J. Phys. B: At. Mol. Phys. **9**, 2561 (1976).
[65] C. A. S. Lima and L. C. M. Miranda, Hydrogen atom in superintense laser fields: Correction to the ground-state energy, Phys. Lett. A **86**, 367 (1981).
[66] Q. Fanyao, A. L. A. Fonseca, and O. A. C. Nunes, Hydrogenic impurities in a quantum well wire in intense, high-frequency laser fields, Phys. Rev. B **54**, 16405 (1996).
[67] F. Y. Qu, A. L. A. Fonseca, and O. A. C. Nunes, Intense laser field effect on confined hydrogenic impurities in quantum semiconductors, Phys. Status Solidi B **197**, 349 (1996).
[68] E. C. Valadares, Resonant tunneling in double-barrier heterostructures tunable by long-wavelength radiation, Phys. Rev. B **41**, 1282 (1990).
[69] M. Fujita, T. Toyoda, J. C. Cao, and C. Zhang, Induced charge-density oscillation under a quantizing magnetic field and intense terahertz radiation, Phys. Rev. B **67**, 075105 (2003).
[70] E. Ozturk, H. Sari, and I. Sokmen, Electric field and intense laser field effects on the intersubband optical absorption in a graded quantum well, J. Phys. D: Appl. Phys. **38**, 935 (2005).
[71] A. L. A. Fonseca, M. A. Amato, and O. L. C. Nunes, Intense field effects on impurities in semiconductors, Phys. Status Solidi B **186**, K57 (1994).

[72] F. M. S. Lima, M. A. Amato, O. A. C. Nunes, A. L. A. Fonseca, B. G. Enders, and E. F. da Silva, Unexpected transition from single to double quantum well potential induced by intense laser fields in a semiconductor quantum well, J. Appl. Phys. **105**, 123111 (2009).
[73] R. D. Mattuk, *A Guide to Feynman Diagrams in the Many-Body Problem* (McGraw-Hill, New York, 1976).
[74] A. P. Jauho and K. Johnsen, Dynamical Franz-Keldysh Effect, Phys. Rev. Lett. **76**, 4576 (1996).
[75] R. Winkler, *Spin-orbit Coupling Effects in Two-dimensional Electron and Hole Systems* (Springer, New York, 2003).
[76] W. Wang, X. M. Li, and J. Y. Fu, Two distinct regimes for the electrical control of the spin-orbit interaction in GaAs wells, J. Magn. Magn. Mater. **411**, 84 (2016).
[77] T. Koga, Y. Sekine, and J. Nitta, Experimental realization of a ballistic spin interferometer based on the Rashba effect using a nanolithographically defined square loop array, Phys. Rev. B **74**, 041302(R) (2006).
[78] I. Vurgaftman, J. R. Meyer, and L. R. Ram-Mohan, Band parameters for III–V compound semiconductors and their alloys, J. Appl. Phys. **89**, 5815 (2001).
[79] A. J. A. Beukman, F. K. de Vries, J. van Veen, R. Skolasinski, M. Wimmer, F. Qu, D. T. de Vries, B. M. Nguyen, W. Yi, A. A. Kiselev, M. Sokolich, M. J. Manfra, F. Nichele, C. M. Marcus, and L. P. Kouwenhoven, Spin-orbit interaction in a dual gated InAs/GaSb quantum well, Phys. Rev. B **96**, 241401(R) (2017).
[80] I. Knez, R. R. Du, and G. Sullivan, Evidence for helical edge modes in inverted InAs/GaSb quantum wells, Phys. Rev. Lett. **107**, 136603 (2011).
[81] W. Wang and J. Y. Fu, Temperature dependence of the Rashba and Dresselhaus spin–orbit interactions in GaAs wells, Phys. B (Amsterdam) **482**, 14 (2016).
[82] B. McNeil and N. Thompson, X-ray free-electron lasers, Nat. Photonics **4**, 814 (2010).
[83] N. Picqué and T. W. Hänsch, Frequency comb spectroscopy, Nat. Photonics **13**, 146 (2019).
[84] J. M. S. Orr, A. M. Gilbertson, M. Fearn, O. W. Croad, C. J. Storey, L. Buckle, M. T. Emeny, P. D. Buckle, and T. Ashley, Electronic transport in modulation-doped InSb quantum well heterostructures, Phys. Rev. B **77**, 165334 (2008).
[85] Y. Y. Liu, B. L. Li, S. Z. Chen, X. W. Jiang, and K. Q. Chen, Effect of room temperature lattice vibration on the electron transport in graphene nanoribbons, Appl. Phys. Lett. **111**, 133107 (2017).
[86] H. Zimmermann, S. Patchkovskii, M. Ivanov, and U. Eichmann, Unified time and frequency picture of ultrafast atomic excitation in strong laser fields, Phys. Rev. Lett. **118**, 013003 (2017).
[87] T. Ando, A. Iwasaki, and K. Yamanouchi, Strong-field fourier transform vibrational spectroscopy of d_2^+ using few-cycle near-infrared laser pulses, Phys. Rev. Lett. **120**, 263002 (2018).
[88] Z. R. Wei, J. L. Li, L. Wang, S. T. See, M. H. Jhon, Y. F. Zhang, F. Shi, M. H. Yang, and Z. H. Loh, Elucidating the origins of multimode vibrational coherences of polyatomic molecules induced by intense laser fields, Nat. Commun. **8**, 1 (2017).
[89] M. E. Corrales, J. González-Vazquez, G. Balerdi, I. R. ISolá, R. de Nalda, and L. Banares, Control of ultrafast molecular photodissociation by laser-field-induced potentials, Nat. Chem. **6**, 785 (2014).
[90] M. Fushitani, C.-N. Liu, A. Matsuda, T. Endo, Y. Toida, M. Nagasono, T. Togashi, M. Yabashi, T. Ishikawa, Y. Hikosaka, T. Morishita, and A. Hishikawa, Femtosecond two-photon rabi oscillations in excited he driven by ultrashort intense laser fields, Nat. Photonics **10**, 102 (2016).
[91] A. Gonoskov, A. Bashinov, I. Gonoskov, C. Harvey, A. Ilderton, A. Kim, M. Marklund, G. Mourou, and A. Sergeev, Anomalous radiative trapping in laser fields of extreme intensity, Phys. Rev. Lett. **113**, 014801 (2014).
[92] S.-W. Bahk, P. Rousseau, T. A. Planchon, V. Chvykov, G. Kalintchenko, A. Maksimchuk, G. A. Mourou, and V. Yanovsky, Generation and characterization of the highest laser intensities (10^{22}W/cm^2), Opt. Lett. **29**, 2837 (2004).
[93] N. Nilforoushan, T. Apretna, C. Song, T. Boulier, J. Tignon, S. Dhillon, M. Hanna, and J. Mangeney, Ultra-broadband THz pulses with electric field amplitude exceeding 100 kV/cm at a 200 kHz repetition rate, Opt. Express **30**, 15556 (2022).
[94] T. Taguchi, T. M. Antonsen, and H. M. Milchberg, Resonant Heating of a Cluster Plasma by Intense Laser Light, Phys. Rev. Lett. **92**, 205003 (2004).
[95] P. Neumayer, B. Aurand, R. A. Costa Fraga, B. Ecker, R. E. Grisenti, A. Gumberidze, D. C. Hochhaus, A. Kalinin, M. C. Kaluza, T. Kühl, J. Polz, R. Reuschl, T. Stöhlker, D. Winters, N. Winters, and Z. Yin, Evidence for ultra-fast heating in intense-laser irradiated reduced-mass targets, Phys. Plasmas **19**, 122708 (2012).
[96] F. Bruehl, M. Banjafar, M. Garten, L. G. Huang, B. E. Marré, M. Nakatsutsumi, L. Randolph, T. E. Cowan, U. Schramm, and T. Kluge, Heating in multi-layer targets at ultra-high intensity laser irradiation and the impact of density oscillation, New J. Phys. **25**, 043024 (2023).
[97] T. Apostolova, D. H. Huang, and D. A. Cardimona, Photon-absorption-induced intersubband optical-phonon scattering of electrons in quantum wells, Phys. Rev. B **67**, 205323 (2003).
[98] J. Zhu, S. L. Ban, and S. H. Ha, Phonon-assisted intersubband transitions in wurtzite GaN/In$_x$Ga$_{1-x}$N quantum wells, Chin. Phys. B **21**, 097301 (2012).
[99] H. B. Teng, J. P. Sun, G. I. Haddad, M. A. Stroscio, S. G. Yu, and K. W. Kim, Phonon assisted intersubband transitions in step quantum well structures, J. Appl. Phys. **84**, 2155 (1998).
[100] D. Maryenko, M. Kawamura, A. Ernst, V. K. Dugaev, E. Y. Sherman, M. Kriener, M. S. Bahramy, Y. Kozuka, and M. Kawasaki, Interplay of spin–orbit coupling and Coulomb interaction in ZnO-based electron system, Nat. Commun. **12**, 3180 (2021).
[101] See Supplemental Material at http://link.aps.org/supplemental/10.1103/PhysRevB.108.235429 for more details about all distinct ingredient contributions of the Rashba couplings of the two subbands (see also Ref. [102] therein).
[102] B. A. Lippmann, Ehrenfest's Theorem and Scattering Theory, Phys. Rev. Lett. **15**, 11 (1965).
[103] E. Bernardes, J. Schliemann, M. Lee, J. C. Egues, and D. Loss, Spin-orbit interaction in symmetric wells with two subbands, Phys. Rev. Lett. **99**, 076603 (2007).
[104] G. J. Ferreira, B. Y. Wang, J. J. Fu, and R. Raimondi,

Charge-spin conversion in two-subband quantum wells with conventional and unconventional Rashba spin-orbit coupling, Proc. SPIE **12656**, 126560H (2023).

[105] R. Song, N. Hao, and P. Zhang, Giant inverse Rashba-Edelstein effect: Application to monolayer $OsBi_2$, Phys. Rev. B **104**, 115433 (2021).

[106] R. Noguchi, K. Kuroda, K. Yaji, K. Kobayashi, M. Sakano, A. Harasawa, T. Kondo, F. Komori, and S. Shin, Direct mapping of spin and orbital entangled wave functions under interband spin-orbit coupling of giant Rashba spin-split surface states, Phys. Rev. B **95**, 041111(R) (2017).

[107] M. Lee, M. O. Hachiya, E. Bernardes, J. C. Egues, and D. Loss, Spin Hall effect due to intersubband-induced spin-orbit interaction in symmetric quantum wells, Phys. Rev. B **80**, 155314 (2009).